

Uncertain pedestrian load modeling for structural vibration assessment in footbridge design

Maximilian Schweizer^{a,*}, Marc Fina^a, Werner Wagner^a, Slobodan Kasic^b, Steffen Freitag^a

^a *Karlsruher Institut für Technologie, Institut für Baustatik, Kaiserstr. 12, 76131 Karlsruhe, Germany*

^b *Harrer Ingenieure GmbH, Am Großmarkt 10, 76137 Karlsruhe, Germany*

ARTICLE INFO

Keywords:

Human-induced load
Polymorphic uncertainty
Fourier series
Step frequency
Footbridge
Vibration assessment
Comfort limits
Fuzzy variable
Random variable

ABSTRACT

The request of material savings in bridge constructions leads to the development towards slender and lightweight structures, which are more sensitive to human-induced vibrations caused by walking pedestrians. The resulting accelerations do not endanger the structural safety, but can be perceived as unpleasant for the user and must therefore be restricted within the limit state of serviceability. For this purpose, the guidelines define acceleration intervals, called as “comfort levels” (CL), which evaluate the comfort of the pedestrians, given the maximum acceleration of the bridge. The model for human-induced loads in the design guideline is based on conservative and deterministic simplifications. In particular, the uncertainties in the human gait parameters are neglected. The main objective of this paper is to develop an uncertain load model for walking pedestrians based on Fourier series. The aleatory and epistemic uncertainties in the human gait parameters are quantified with appropriate uncertainty models relying on available data. In a dynamical finite element analysis, the model is used to simulate groups of pedestrians randomly walking over a bridge to calculate the resulting acceleration amplitudes. The approach is applied to a single span beam and to a real world footbridge using a 3D finite element model. The results are then evaluated within the CLs, enabling new assessment methods.

1. Introduction

The trend towards lightweight structures in bridge constructions causes modern footbridges to be more sensitive to human-induced vibrations caused by walking pedestrians. An inappropriate consideration of human-induced vibrations can lead to unacceptable accelerations and thus to significant financial loss, such as in the case of the London Millennium Bridge in 2000 [1]. The design guideline DIN EN 1991-2 [2] defines acceleration intervals called as “comfort levels” (CL) to restrict the vibrations in the limit state of serviceability. The load model from the design guideline uses deterministic values based on conservative assumptions. The step frequency of the pedestrians is assumed to be equivalent to the structural eigenfrequency, which causes resonance effects representing the worst case scenario. The load model is a distributed load over the bridge surface defined as cosine function. In this way the pedestrians are not considered as single independent loads, but as a homogeneous group. During the last decades new load models for pedestrian-induced vibrations based on experimental data have been developed. It has been shown, that the load function of a single pedestrian can be described with a Fourier series containing four to five harmonics [3–8]. For the Fourier coefficients, which are called as

“dynamic load factors” (DLF_i) in the context of human-induced loads, and the phase shifts φ_i , different authors present different values. Thus, it is not clear, which Fourier series is the most appropriate to describe human-induced loads realistically. Some of the dynamic load factors show a correlation with the step frequency f_s . Therefore, the step frequency is used as the main parameter to describe the human gait. The step frequency of pedestrians entail a special variability, which cannot be uniformly defined, but is dependent on individual physiological and psychological characteristics, such as body dimensions, body weight, gender, age, state of mind and purpose of travel. In [9,10] it is shown, that even the economic and social status of an individual has an influence on his walking speed. In addition, it turns out that high population and the strong economic development of a country also has a positive correlation with the mean walking speed of the population [11–13]. Aside from the individual characteristics just mentioned, environmental factors can also influence the gait. This includes, e.g., the weather, the brightness, the attractiveness of the surroundings, the slope, the flooring, the density of people and oncoming traffic.

In order to account for the aleatory uncertainty in the pedestrians parameters, most authors use normal distributed random variables

* Corresponding author.

E-mail address: maximilian.schweizer@kit.edu (M. Schweizer).

whose probability distributions come from laboratory experiments or field observations on real bridges. It is implicitly assumed that the parameters generated in this way are universally applicable. In reality, there can be significant differences in the parameters depending on the situation, hence the transfer of observed gait parameters to other situations can be unrealistic. The realistic modeling of pedestrian groups consisting of people with randomly distributed characteristics is a particularly complex task. Since different authors assume different probability distributions, it is not possible to define one universal distribution. The lack of knowledge about the “true” parameters, is called as epistemic uncertainty and can be quantified as fuzzy or interval variable [14,15].

Taking both the aleatory and the epistemic uncertainty into account leads to the concept of polymorphic uncertainty, according to [16], also known as imprecise probability. Some examples for the application of polymorphic uncertainties in structural engineering problems are: crack propagation and optimization of a reinforced concrete bridge [17], scattering material properties of wood [18], shell buckling [19–22], seismic performance of buildings [23], analysis of dynamical processes [16,24], a concept for data-driven computational mechanics [25] and earth structure assessment [26] among many others. In [27] different polymorphic uncertainty quantification approaches are compared within a benchmark example for the reliability assessment and optimization-based design of a steel frame structure. The aleatory uncertainty in human-induced vibrations of footbridges has been considered in many research projects, see, for example, [4,6,28–34]. The main objective in this paper is the development of a new load model considering polymorphic uncertainty and the implementation into a finite element model in order to calculate human-induced vibrations on footbridges caused by walking pedestrians. The uncertainty in the pedestrian parameters is quantified with an uncertainty model based on experimental data from the literature. The pedestrians step frequency is modeled as a normal distributed random variable with a fuzzy mean value and a fuzzy standard deviation which leads to the fuzzy probability based random (fp-r) variable. The Fourier parameters are modeled as fuzzy variables. In this paper, the fuzzy-stochastic analysis is a three-loop computational model consisting of the deterministic FE-model, the Monte-Carlo simulation (MCS) and the α -Level optimization (ALO). Because of the high computational effort, the MCS is replaced with a surrogate model based on least square polynomials. In conclusion, the comfort level of the bridge is evaluated with recommendations from the design guideline. The highlights of this paper can be summarized as follows:

- (1) Uncertainty quantifications for human-induced loads
- (2) Introduction of a fuzzy Fourier load model for walking pedestrians
- (3) Simulation of human-induced vibrations of a real world footbridge with polymorphic uncertain data
- (4) New assessment methods for the footbridges comfort level

2. Uncertainty modeling

In this section, the basic concepts of the used uncertainty models are summarized. Uncertainty can be divided into aleatory and epistemic uncertainty [14,15]. Aleatory uncertainty describes the randomness of an experiment and is modeled in general as random variable. Epistemic uncertainty describes the lack of information about a parameter and can be modeled as interval variable or as fuzzy variable. In the following, the three basic uncertainty models: random variable, interval variable and fuzzy variable are explained, see Fig. 1. Finally, the combination of aleatory and epistemic uncertainties, i.e., the polymorphic uncertainty is introduced and the corresponding uncertainty model is presented.

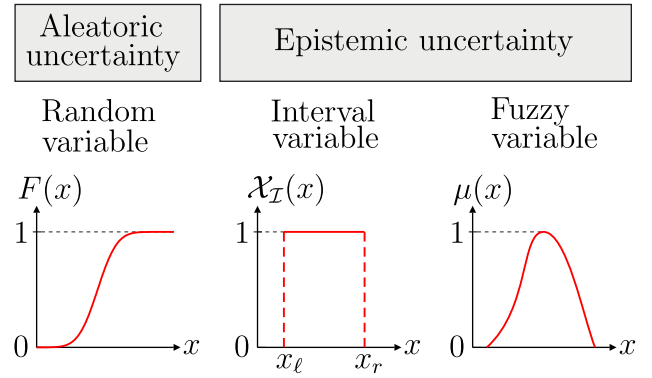


Fig. 1. Three basic uncertainty models: cumulative distribution function of a random variable (left), interval variable (center), membership function of a fuzzy variable (right).

2.1. Random variable

A random variable is defined in the probability space (Ω, Σ, P) , which is composed of a set of elementary events Ω , a σ -algebra Σ and a probability measure P . The random variable X is a mapping operator, which assigns every result $\omega \in \Omega$ to a real number $X(\omega)$

$$X : \Omega \rightarrow \mathbb{R}, \omega \mapsto X(\omega) . \quad (1)$$

The probability measure $P \in [0, 1]$ is defined with the probability density function (PDF) $f(x)$ and the cumulative distribution function (CDF) $F(x)$. The CDF is the integral of the PDF

$$F(x) = P(X \leq x) = \int_{-\infty}^x f(t) dt . \quad (2)$$

Where $P(X \leq x)$ is the probability, that the random variable X takes on a value less or equal to x and is called “non-exceedance probability”. The specification of a non-exceedance probability p or exceedance probability $1 - p$ is referred to as quantile value. The number x_p is a p -quantile of P , if

$$P(X \leq x_p) \geq p \quad \text{and} \quad P(X \geq x_p) \geq 1 - p . \quad (3)$$

A p -quantile divides a probability distribution in a left part with probability p and a right part with probability $1 - p$. The 50%-quantile is the median and, in the case of a symmetric distribution, it coincides with the mean value. The random variables used in this paper are, e.g., the pedestrians step frequency and body weight, time delay between pedestrians, material stiffness and density.

2.2. Interval and fuzzy variables

An interval $I \in \mathbb{R}$ is a set that contains all real numbers lying between two interval limits $x_l < x_r \in \mathbb{R}$. The membership of an element x to an Interval I is whether true or false, which can be expressed with the characteristic function

$$\mathcal{X}_I = \begin{cases} 1, & x \in I \\ 0, & x \notin I \end{cases} . \quad (4)$$

A fuzzy variable is an extension of an interval variable. The interval variable is referred to as “crisp” set, in order to distinguish it from the fuzzy set. In the fuzzy-set-theory, the membership of an element x to a set A is rated gradually with the membership function $\mu_A(x)$. The normalized fuzzy variable \tilde{A} is defined as

$$\tilde{A} = \{(x, \mu_A(x)) | x \in \mathbb{R}\} \\ \mu_A(x) : \mathbb{R} \rightarrow [0, 1] . \quad (5)$$

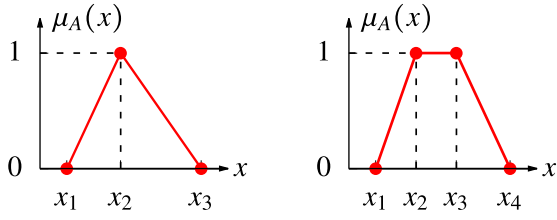


Fig. 2. Fuzzy triangular number (left) and fuzzy trapezoidal interval (right).

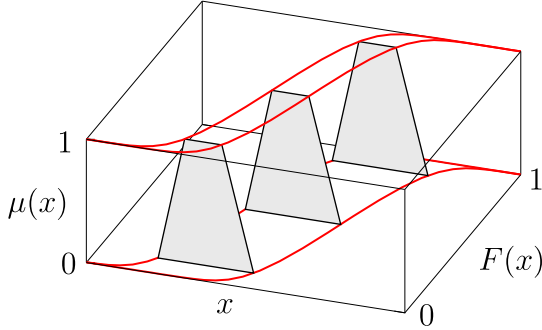


Fig. 3. Fuzzy CDF of a fuzzy probability based random variable.

If the membership function $\mu_A(x)$ of a fuzzy variable is monotonically decreasing on both sides from the maximum value $\mu_A(x) = 1$, the fuzzy variable is convex and defined as

$$\begin{aligned} \mu_A(x_2) &\geq \min[\mu_A(x_1); \mu_A(x_3)] \quad , \\ \forall x_1, x_2, x_3 &\in \tilde{A} \quad \text{with} \quad x_1 \leq x_2 \leq x_3 \quad . \end{aligned} \quad (6)$$

The fuzzy variables used in this paper are the Fourier parameters as fuzzy triangular numbers and the stochastic distribution parameters of the step frequency as fuzzy trapezoidal intervals, which are convex and linear, as shown in Fig. 2. Both fuzzy variables are described by the following notation:

- fuzzy triangular number: $\tilde{A} = \langle x_1 \ x_2 \ x_3 \rangle$
- fuzzy trapezoidal interval: $\tilde{A} = \langle x_1 \ x_2 \ x_3 \ x_4 \rangle$

2.3. Fuzzy probability based random variable

Polymorphic uncertainty emerges from the combination of aleatory and epistemic uncertainties and is quantified in this paper as fuzzy probability based random (fp-r) variable, which is defined in the fuzzy probability space $(\Omega, \Sigma, \hat{P})$. The fuzzy probability $\hat{P} = (\hat{P}_\alpha)_{\alpha \in (0,1]}$ assigns every $A \in \Sigma$ on every alpha-level to a probability measure in form of an interval $\hat{P}_\alpha = [\hat{P}_{\alpha,l}, \hat{P}_{\alpha,r}]$

$$0 \leq \hat{P}_{\alpha,l}(A) \leq \hat{P}_{\alpha,r}(A) \leq 1 \quad . \quad (7)$$

For every alpha-level, an interval of CDFs is defined as

$$F_X = ((F_X)_\alpha)_{\alpha \in (0,1]} \quad . \quad (8)$$

Polymorphic uncertainty can be used, if the expected value $E[x]$ or the standard deviation σ_x of a random variable is uncertain. This is the case, for example, if the stochastic distribution parameters from several independent measurement studies are given but the samples are not available. Each measurement study enables the description of a random variable, but with different expected values $E[x]$ and standard deviations σ_x for each measurement. Defining a crisp random distribution from these measurements is only possible if enough samples are available. In most cases, however, they differ from campaign to campaign due to the small sample size or the boundary conditions of the measurements. The lack of knowledge about the entirety of the samples is the epistemic uncertainty, which can be modeled with interval

or fuzzy variables. The combination of random and interval variables leads to the p-box representation, while the combination of random and fuzzy variables leads to the fp-r variable, which is an extension of the parametric p-box representation, as it assigns a parametric p-box to each value of the membership function $\mu(x)$. With a few data the uncertainty quantification can be improved and is particularly useful for highly sensitive parameters. If only the bounds are of interest, a p-box approach is sufficient. The representation of the fp-r variable is referred to as fuzzy CDF and is shown in Fig. 3. In this paper, the pedestrians step frequency is modeled with an fp-r variable, which is introduced in Section 4.1.

3. Numerical structural analysis with uncertain data

In this section, the implementation of fuzzy, random and fp-r variables in a numerical structural analysis program is explained based on [14,19,35]. The dynamic structural analysis consists of solving the equation of motion

$$\mathbf{M}\ddot{\mathbf{v}}(t) + \mathbf{D}\dot{\mathbf{v}}(t) + \mathbf{K}\mathbf{v}(t) = \mathbf{P}(t) \quad (9)$$

with mass matrix \mathbf{M} , damping matrix \mathbf{D} , stiffness matrix \mathbf{K} and load vector $\mathbf{P}(t)$. The damping matrix is modeled with a Rayleigh-damping: $\mathbf{D} = \alpha\mathbf{M} + \beta\mathbf{K}$. The structure is modeled in a Finite Element Analysis Program (FEAP [36]) and Eq. (29) is solved with the implicit Newmark method [37], which is a common time integration method used in dynamic structural analysis. With that, the structural acceleration of each FE-node is calculated in each time step t_n . The dynamic structural analysis with fuzzy and random input variables leads to a fuzzy stochastic process, where a fp-r output variable is defined for every timestep t_n . A fuzzy stochastic process is illustrated in Fig. 4, where x and z are the input and the output variable respectively. For each sample point x of the fuzzy input space a stochastic process $z(t)$ takes place. At each timestep t_n of the stochastic processes, a probability distribution of the output z is defined. The probability distribution yields a specific quantile value as input for the α -Level optimization (ALO), which results in the fuzzy quantile value of the fp-r output variable. Repeating the ALO for a discretization of quantile values, yields the fuzzy CDF representation. In Fig. 4, the principle is shown exemplary for the 95%-quantile value. The concept of α -Level optimization is explained later in this section.

The numerical structural analysis with fuzzy and random variables is realized with a three-loop computational model consisting of the deterministic FE-model, the Monte-Carlo-Simulation (MCS) and the α -Level optimization (ALO). The computational model is shown in Fig. 5 (left). The fuzzy input variables \tilde{x} are mapped to the fuzzy output variables \tilde{z} with the ALO and the mapping operator $\mathcal{M}(x)$

$$x \in D \subset \mathbb{R}^M \mapsto z = \mathcal{M}(x) \in \mathbb{R}^1 \quad . \quad (10)$$

In this paper, the mapping operator $\mathcal{M}(x)$ represents the Monte Carlo Simulation (MCS) to obtain a stochastic quantity of interest as the output z , e.g., the mean value, standard deviation or a specific quantile value. Because of the high computational effort, the MCS is replaced with a surrogate model, see for example [21,38–41]. Alternatively, a surrogate modeling for the deterministic FE-model and the ALO could also be taken into consideration, see, for example, the multilevel surrogate modeling approach according to [42]. In the presented application, the uncertain input variables for the MCS are, for example, the mean value and standard deviation of the pedestrians step frequency and the Fourier parameters of the pedestrians load function. The output of the deterministic FE-model is the maximum acceleration a_{\max} of the footbridge. The output of the MCS is defined as the 95%-quantile value of a_{\max} , see Fig. 5 (right), but can be in general any stochastic quantity of a_{\max} , e.g., mean or standard deviation.

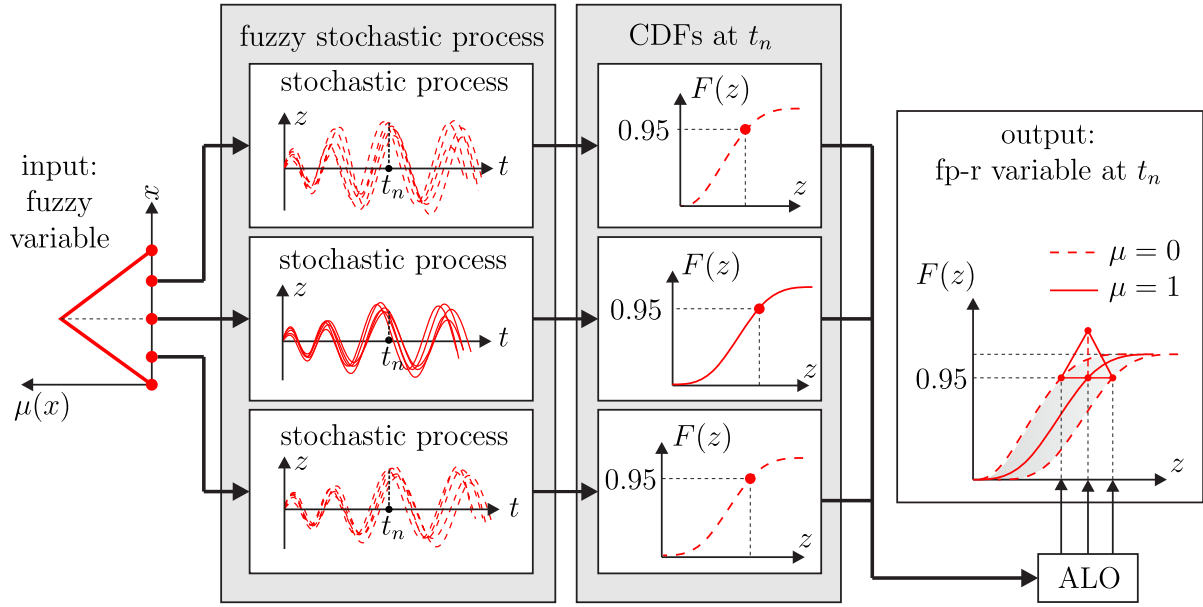


Fig. 4. Fuzzy stochastic process and definition of an fp-r variable at each timestep t_k with the ALO.

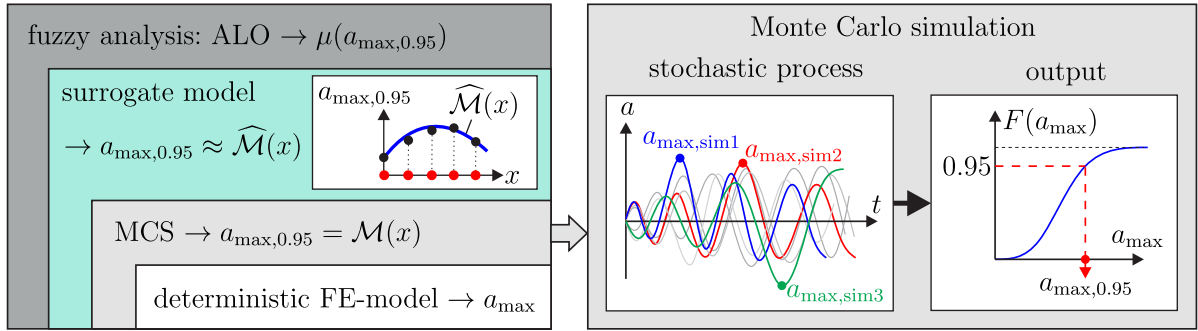


Fig. 5. Three-loop computational model for the fuzzy-stochastic analysis (left) and Monte Carlo Simulation of the stochastic process(right).

For the numerical implementation of fuzzy variables in a computational model, the membership function is divided in alpha-levels:

$$A_{\alpha_k} = \{x \in \mathbb{R} \mid \mu_A(x) \geq \alpha_k\}, \quad \alpha \in (0, 1], \quad k = 1, 2, \dots, N_{\text{alev}}. \quad (11)$$

This procedure is referred to as alpha-level discretization, see [35]. Each alpha-level is an interval $A_{\alpha_k} = [x_{\alpha_k,l}, x_{\alpha_k,r}]$ with the membership $\mu = \alpha_k$. The support $S(\tilde{A})$ is the interval on the bottom alpha-level and contains all elements of A

$$S(\tilde{A}) = \{x \in \mathbb{R} \mid \mu_A(x) > 0\}. \quad (12)$$

In order to obtain the fuzzy output variable \tilde{z} , the minimum and the maximum output values of $\mathcal{M}(x)$ are searched on each alpha-level. The minimum output results in the left bound $z_{\alpha_k,l}$ and the maximum output results in the right bound $z_{\alpha_k,r}$ of the fuzzy output variable \tilde{z}

$$z_{\alpha_k,l} = \min[\mathcal{M}(x)] \quad \text{and} \quad z_{\alpha_k,r} = \max[\mathcal{M}(x)] \quad \forall x \in A_{\alpha_k} \quad (13)$$

with $k = 1, 2, \dots, N_{\text{alev}}$.

This extreme value problem is referred to as α -level optimization (ALO). The MCS takes place on the sample points on the support $S(\tilde{A})$. In every MCS the FE-model solution is computed N times and the specific stochastic parameter z is estimated based on the samples. After the MCS has been realized at each sample point, the ALO takes place searching for the extremal output values on every alpha-level. The numerical

treatment of the fuzzy-stochastic analysis is a combination of the ALO as outer loop and the MCS as inner loop. For a sufficient precise estimation of the considered stochastic parameter, it is important to execute enough realizations of the MCS which is computationally expensive.

In order to reduce the computational effort, a surrogate model $\hat{\mathcal{M}}(x)$ is used to replace the MCS. Therefore, the MCS is realized on a few sample points $\mathcal{X}_{\text{sim}} = \{x_1, \dots, x_{N_{\text{sim}}}\} \subset D$, to obtain the output variables $\mathcal{Z}_{\text{sim}} = \{z_1, \dots, z_{N_{\text{sim}}}\} \in \mathbb{R}$. With the output data, the surrogate model is generated as approximated function $\hat{\mathcal{M}}$ on the support. The ALO is then applied on the surrogate model:

$$\hat{z}_{\alpha_k,l} = \min[\hat{\mathcal{M}}(x)] \quad \text{and} \quad \hat{z}_{\alpha_k,r} = \max[\hat{\mathcal{M}}(x)] \quad \forall x \in A_{\alpha_k} \quad (14)$$

with $k = 1, 2, \dots, N_{\text{alev}}$.

On every alpha-level, the domain $D = \{x \mid x \in A_{\alpha_k}\}$ is adjusted, so that the surrogate model has to be generated only once. The ALO using a surrogate model on the support is represented in Fig. 6. The ALO and the surrogate modeling can be repeated for a discretization of different quantile values, in order to obtain the fp-r output variable, which can be represented as fuzzy CDF.

For problems with high stochastic scattering, the least square (LSQ) method [43] is recommended to approximate the surrogate model. The LSQ method builds a polynomial function based on the least square error of a few sample points, where the MCS has to take place. In the case of a fullfactorial design of experiments (DoE), the total number of sample points N_{sim} , is calculated as exponential function $N_{\text{sim}} = n^M_{\text{sim}}$.

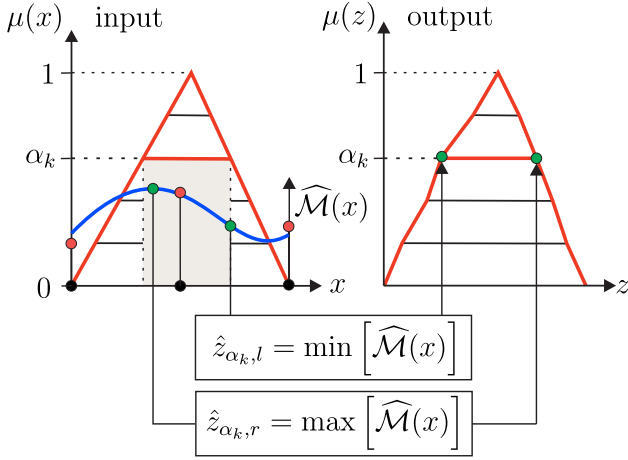


Fig. 6. Representation of the ALO on the α_k using a surrogate model $\widehat{\mathcal{M}}(x)$ on the support of a fuzzy input triangle number.

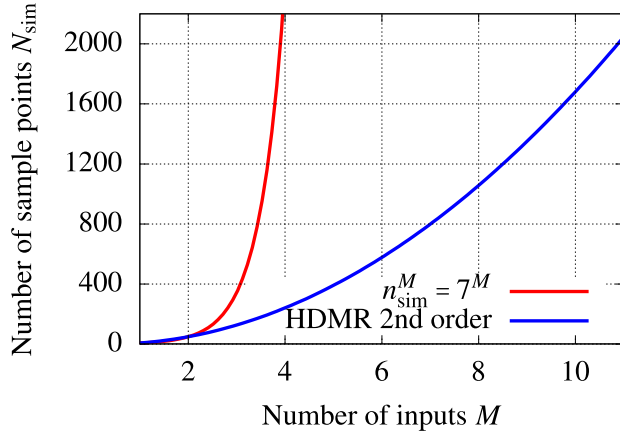


Fig. 7. Representation of the number of sample points according to [19].

Whereby M is the number of input variables and n_{sim} is the number of sample points per dimension. In order to reduce the computational effort when modeling with more than two input variables, the high dimensional model representation (HDMR) is used according to [44, 45]. In this way, the reciprocal influence of the input variables is taken into account up to a degree L . In most cases, the degree of $L = 2$ is sufficient [46,47]. The total number of sample points N_{sim} is calculated with respect to the number of sample points per dimension n_{sim} and the number of input variables M according to [46]

$$N_{\text{sim}}(M, n_{\text{sim}}) = \sum_{i=0}^L \frac{M!}{i!(M-i)!} (n_{\text{sim}} - 1)^i \quad (15)$$

The computational effort for a number of sample points per dimension of $n_{\text{sim}} = 7$ with respect to the number of inputs M is represented in Fig. 7. With the cut-HDMR-method, cutting lines and cut surfaces are generated through a reference point in the center of the input space. The generated cut functions are LSQ-polynomials. The ALO is then applied on the polynomial functions to find the extremal solutions on every α -level. The optimization strategy used in this paper is the particle swarm optimization, from Kennedy and Eberhart [48].

4. Human-induced loads

The human form of movement is divided in walking and running. Running is generally less common than walking. In addition, people who run are less sensitive to noticeable vibrations because they

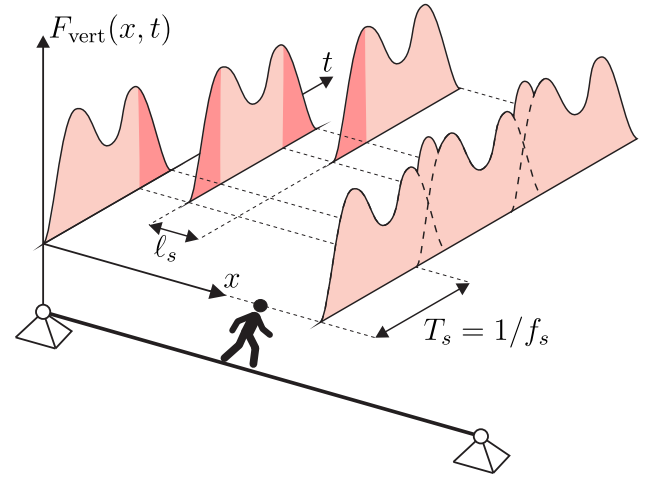


Fig. 8. Representation of human-induced loads in the vertical direction.

are consciously concentrated on their movement. For these reasons, running is usually less important from a structural dynamic point of view and is comparatively rarely found in scientific studies [32]. Therefore, this paper concentrates on investigating the walking form of movement. During walking, a pedestrian produces a dynamic time varying force, which has components in all three directions: vertical, lateral and longitudinal [3]. The vertical component is regarded as the most significant due to its higher amplitude, resulting in extensive investigations. A walking pedestrian has constant contact with the ground with alternating single and double stance phases (ssp and dsp). In the dsp, the vertical load of a single step is overlapped with the load of the next step. The vertical load-time histories of three consecutive steps and their superposition is represented exemplary in Fig. 8. The distance and the time delay between two consecutive steps are the step length ℓ_s and the step period T_s . The step frequency f_s , as the reciprocal value of the step period, is the number of steps per second and is measured in Hertz [Hz]. Many studies confirm that the total dynamic load of a walking pedestrian is nearly periodic [3–8,49,50]. The load function is therefore described in many publications with the Fourier series

$$F_{\text{vert}}(t) = G \cdot \left(1 + \sum_{i=1}^n DLF_{i,\text{vert}} \sin(2\pi \cdot i \cdot f_s \cdot t - \varphi_{i,\text{vert}}) \right) \quad (16)$$

Here, G is the pedestrians weight [N], DLF_i is the dynamic load factor (Fourier coefficient) of the i th harmonic, f_s is the step frequency [Hz], φ_i is the phase shift of the i th harmonic, i is the order number of the harmonic and n is the total number of contributing harmonics. As the DLFs become smaller with increasing harmonic i , they are practically negligible above a certain harmonic n . The number n of considered harmonic components varies in the literature. One of the first authors using a Fourier series for human-induced loads is Bachmann [49,50], considering three harmonics. Various authors investigated the walking pattern of pedestrians in order to find an appropriate way to describe the parameters. Thus, a large amount of different information is available. In the following two subsections, the information from the literature about gait and load parameters is presented, in order to develop an uncertainty model for human-induced loads on footbridges.

4.1. Gait parameters

The gait parameters are the step frequency f_s [Hz], the velocity v_s [m/s²], the period T_s [s] and the step length ℓ_s [m]. The relationship between walking speed v_s and step frequency f_s is recommended in SYNPEX [5] to

$$v_s = 1.271 \cdot f_s - 1 \text{ [m/s]} \quad (17)$$

Table 1
Normal distribution of step frequencies f_s [Hz] according to [54].

Gender	Footbridge	$E[f_s]$	σ_{f_s}
Women	Merchant	1.89	0.11
	Lowry	1.84	0.10
Men	Merchant	1.84	0.11
	Lowry	1.76	0.086

Table 2
Normal distribution for the step frequency according to [56].

Age/gender	Mean value $E[f_s]$			std. deviation σ_{f_s}		
	slow	norm.	fast	slow	norm.	fast
$a < 40$						
Men	1.48	1.80	2.03	0.19	0.18	0.14
Women	1.49	1.88	2.13	0.11	0.11	0.08
$40 < a < 60$						
Men	1.52	1.81	2.02	0.19	0.14	0.14
Women	1.52	1.87	2.12	0.15	0.12	0.17
$a > 60$						
Men	1.51	1.78	1.95	0.11	0.10	0.11
Women	1.53	1.94	2.16	0.18	0.12	0.14

Here, the step frequency is used as main gait parameter, while the remaining parameters are determined with respect to f_s . Numerous authors [31,32,49,51–56] carry out measurements and determine the step frequency f_s as normal distributed, giving indications for the mean value $E[f_s]$ and the standard deviation σ_{f_s} . Some of the authors measured on real bridges while others used a constructed setup. An example for a measurement on a real footbridge is described in Pachi and Ji [54], who observed 100 women and 100 men on the Merchant footbridge in London and the Lowry bridge in Manchester. The pedestrians did not know, that they were observed. In this way psychological influence is excluded. The parameters determined in [54] are given in Table 1. An example for a constructed setup is found in Butz [56], who used a constructed 12 m long platform, which is able to vibrate horizontally. The testgroup of 100 people crossed the platform in three different walking intentions: “slow”, “normal” and “fast”. The results from [56], divided in the categories: gender, age and walking intention, are shown in Table 2. In Petersen [55] two separate measurement campaigns on a real footbridge are given, one with 55 pedestrians and one with 50 pedestrians. The results from both measurements are presented separately in Table 3. Sahnaci [32] used a platform construction in a university workshop with a group of 38 women and 189 men. The test subjects are mainly engineering students which explains the small proportion of female participants in 2008. The walking speed is freely chosen to simulate the natural gait. A measurement campaign with a notably large number of pedestrians is described in Zivanovic [31], where video records of 1976 people crossing over the Podgorica footbridge in Montenegro are analyzed. The results from Zivanovic [31], Sahnaci [32] and many others [49,51–53,55], are presented in Table 3. For modeling a random time delay Δt between two pedestrians when entering the bridge, the Poisson distribution is given in Sahnaci [32]

$$\Delta t = -\frac{1}{\lambda} \cdot \ln(1 - r) \quad (18)$$

with the mean arrival rate λ [pers./s] and the uniformly distributed random number $r \in [0, 1]$. The mean arrival rate λ is

$$\lambda = N_{\text{pers}} \cdot \frac{v_{s,\text{mean}}}{L} \quad (19)$$

with the number of pedestrians N_{pers} , the mean pedestrians velocity in the current simulation $v_{s,\text{mean}}$ [m/s] and the span length L [m].

The large amount of different information from literature shows that different measurement campaigns lead to different results for the stochastic parameters of the step frequency. Possible reasons for these differences are a small sample size and different boundary conditions,

Table 3
Normal distribution of step frequencies f_s [Hz] from [31,32,49,51–53,55].

Literature	Category/situation	$E[f_s]$	σ_{f_s}
Matsumoto [51]	Outside	1.99	0.177
Kramer [52]	–	2.20	0.299
ECSC [53]	Inside	2.00	0.17
Zivanovic [31]	Podgorica bridge	1.87	0.185
Sahnaci [32]	38 women	1.99	0.121
	189 men	1.90	0.122
	Slow	1.7	–
Bachmann [49]	Normal	2.0	–
	Fast	2.3	–
	Normal, 55 pers.	1.77	0.175
Petersen [55]	Normal, 50 pers.	1.75	0.19
	Fast, 55 pers.	2.17	0.205
	Fast, 50 pers.	2.10	0.266

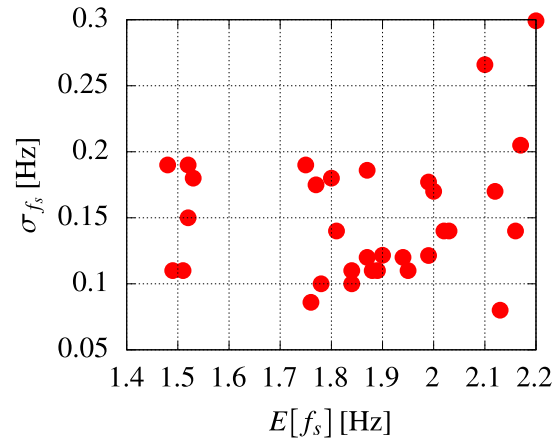


Fig. 9. Correlation plot between the mean value $E[f_s]$ and the standard deviation σ_{f_s} of the step frequency.

which are often unknown. Also dividing the measurements into categories (e.g., gender, age, velocity, situation) shows that each category has its own random distribution. The precise definition of one universal random distribution for the step frequency is not possible. In order to consider both the aleatory and the epistemic uncertainty, in this paper, the step frequency is modeled with a fp-r variable. In order to investigate the correlation between the mean value $E[f_s]$ and the standard deviation σ_{f_s} , all value-pairs are plotted in Fig. 9. As there is clearly no correlation, the two stochastic parameters of the step frequency are modeled as independent fuzzy variables: the fuzzy mean value $\tilde{E}[f_s]$ and the fuzzy standard deviation $\tilde{\sigma}_{f_s}$. The fp-r variable can be expressed with the following notation for the normal distribution: $f_s \sim \mathcal{N}(\tilde{E}[f_s], \tilde{\sigma}_{f_s})$. In order to choose an appropriate fuzzy variable, a visualization in a histogram can be helpful. The values for $E[f_s]$ and σ_{f_s} from literature [31,32,49,51–56] are shown as histogram together with the membership function $\mu(E[f_s])$ and $\mu(\sigma_{f_s})$ in Fig. 10. The support bounds ($\mu = 0$) are determined at the minimum and maximum of the histogram values. The trend values ($\mu = 1$) are the values, that occur most frequently. In general, the choice of the shape of the fuzzy variable depends on the available data. Based on Fig. 10, there appears to be a range of most possible values, which are given the membership $\mu = 1$, leading to a trapezoidal shape.

$$\begin{aligned} \tilde{E}[f_s] &= \langle 1.45 \quad 1.7 \quad 2.05 \quad 2.35 \rangle, \\ \tilde{\sigma}_{f_s} &= \langle 0.08 \quad 0.11 \quad 0.19 \quad 0.3 \rangle. \end{aligned} \quad (20)$$

For the realistic modeling of human induced loads of walking pedestrians, the values for the step frequency f_s should be restricted within limit values in order to ensure the physical plausibility. Therefore, all step frequencies are limited within the bounds $f_{s,\text{min}} \leq f_s \leq f_{s,\text{max}}$ [Hz]. Here, the bounds are chosen as $f_{s,\text{min}} = 1.0$ Hz and $f_{s,\text{max}} = 2.8$ Hz. The step frequency is therefore modeled with a truncated fp-r variable.

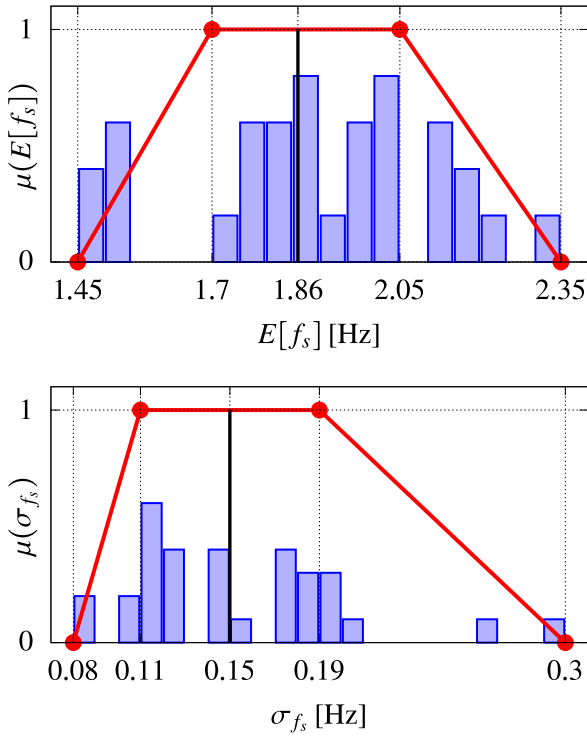


Fig. 10. Membership function μ and histogram for $E[f_s]$ and σ_{f_s} .

4.2. Load parameters

The dynamic load induced by pedestrians is described with the Fourier series according to Eq. (16), whereby the load parameters consist of the pedestrians body weight G [N], the dynamic load factors (Fourier coefficients) DLF_i and the phase shifts φ_i . The dynamic load factors are dimensionless dynamical scaling factors of the pedestrians body weight G . The body weight is modeled with two normal distributed random variables, one for men and one for women. The mean values and standard deviations are $E[G_w] = 71.4$ [kg], $\sigma_{G_w} = 15.1$ [kg] for women and $E[G_m] = 87.0$ [kg], $\sigma_{G_m} = 15.0$ [kg] for men, see [57]. The gender of the pedestrians has a 50% chance to be either male or female and is computed with a uniform distributed random variable.

The Fourier parameters are determined experimentally by measuring the load-time histories of walking pedestrians with force measuring plates placed on the ground and subsequent Fourier transformation. The measurement results from [4–8,31,49] are presented in Tables 4–6 and in Eqs. (21) and (22). The dynamic load factors decrease with higher harmonics, which means that only the first few DLF's need to be considered, while the remaining can be neglected. The number of considered harmonics depends on the considered literature. Most of the authors consider four harmonics and determine the Fourier coefficients in dependency of the step frequency f_s . In particular, the first coefficient DLF_1 has a strong positive correlation with the step frequency f_s . This means that walking faster induces forces with higher amplitudes. According to Bachmann [49,50] the first DLF is piecewise linear, while the remaining load parameters are constants. Seiler&Hüttner [7] determined constant load parameters using special pressure measuring soles used in the orthopedic technology, which are placed in the pedestrians shoes and allowed free movement. In the design guideline from ISO 10137 [8] five harmonics are considered. The first DLF is linear, while the remaining DLFs are constants and the phase shifts are all zero. The parameters according to Bachmann [49], Seiler&Hüttner [7] and ISO 10137 [8] are given in Table 4. An example for the use of random variables for the Fourier parameters is given in

Table 4
Vertical load parameters for walking according to Seiler&Hüttner [7].

	Bachmann	Seiler&Hüttner	ISO 10137
DLF_1	0.4, $f_s \leq 2.0$ Hz 0.5, $f_s \geq 2.4$ Hz ^a	0.4	$0.37 \cdot (f_s - 1)$
DLF_2	0.1	0.15	0.1
DLF_3	0.1	0.10	0.06
DLF_4	0	0.05	0.06
DLF_5	0	0	0.06
φ_1	0	$\pi/2$	0
φ_2	$\pi/2$	$-\pi \cdot 5/6$	0
φ_3	$\pi/2$	$\pi/2$	0
φ_4	0	$-\pi \cdot 5/6$	0
φ_5	0	0	0

^a Linear interpolation is used for $2.0 < f_s < 2.4$.

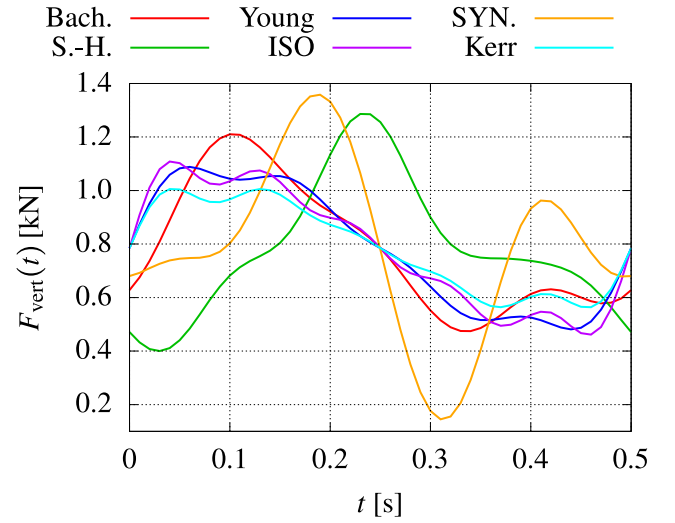


Fig. 11. Fourier series for the vertical load $F_{\text{vert}}(t)$ [kN] according to [4–8,49] with an exemplary step frequency of $f_s = 2.0$ Hz and body weight of 80 kg, plotted regarding to the time period $T = 0.5$ [s].

Table 5
Normal distribution of the vertical DLFs for walking according to [6].

i	Mean value $E[DLF_i]$	Standard deviation σ_{DLF_i}
1	... see Eq. (21) ...	
2	0.07	0.03
3	0.05	0.02
4	0.05	0.02
5	0.03	0.015

Kerr [6], where 1000 force records from 40 test persons are collected to determine the mean value and the standard deviation for the DLFs considering five harmonics. For the first DLF, the mean value $E[DLF_1]$ is a third degree polynomial function of f_s and the standard deviation σ_{DLF_1} is dependent from the mean value

$$E[DLF_1] = -0.2649 \cdot f_s^3 + 1.3206 \cdot f_s^2 - 1.7597 \cdot f_s + 0.7613$$

$$\sigma_{DLF_1} = 0.16 \cdot E[DLF_1] \quad (21)$$

The remaining parameters, according to [6], are given in Table 5. Young [4] presented a comparison of the DLFs from Kerr and many others and derived 50%- and 25% exceedance probabilities for the DLFs, see Table 6. In SYNPEX [5] all four DLFs and phase shifts are second and third degree polynomial functions of the step frequency f_s

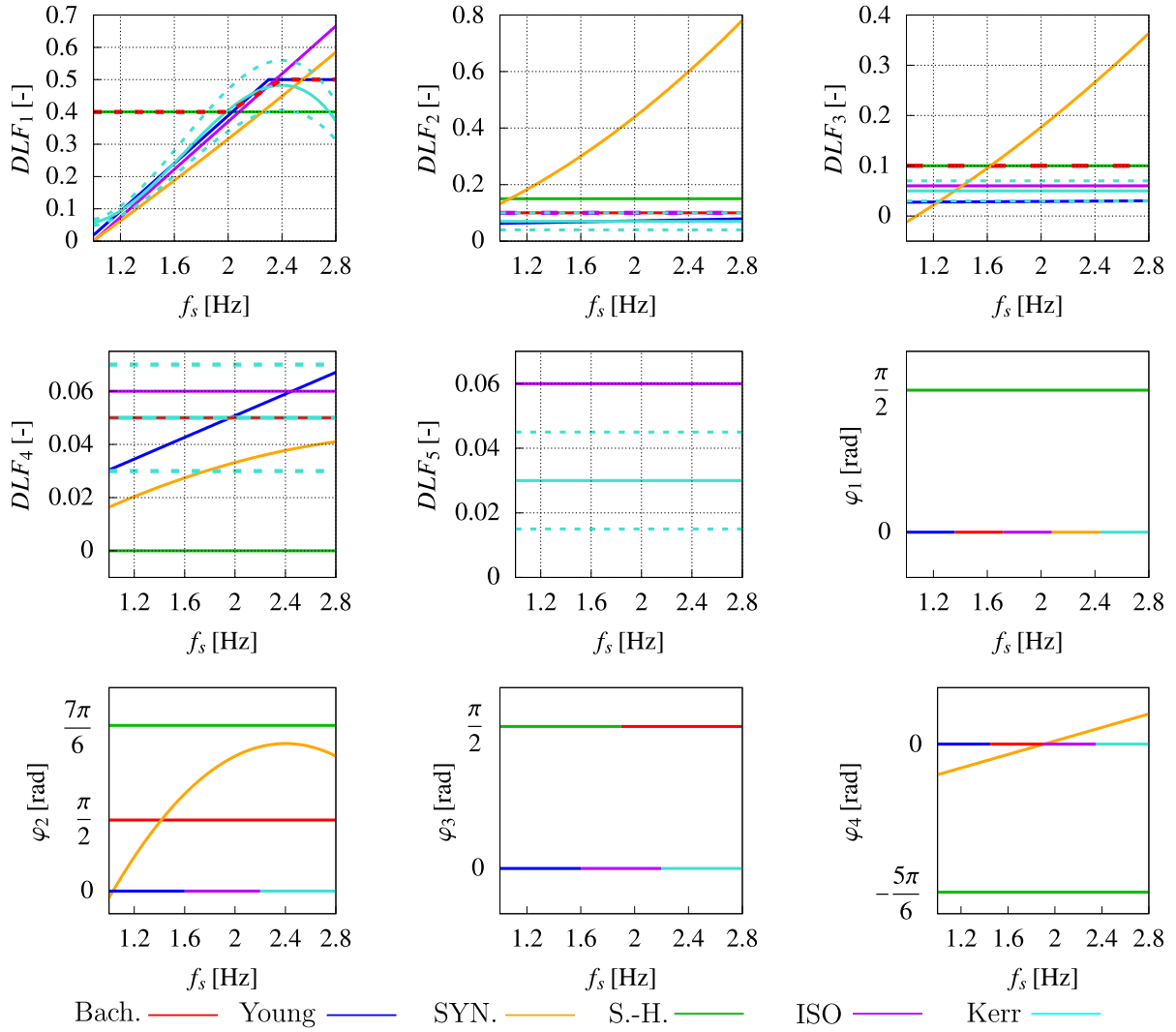


Fig. 12. Dynamic load factors DLF_i and phase shifts φ_i of the Fourier series from the six different literature sources up to the fifth harmonic.

Table 6

Vertical DLFs for walking according to Young [4].

	Exceedance probability	
	50%	25%
DLF_1	$0,37 \cdot (f_s - 0,95) \leq 0,5$	$0,41 \cdot (f_s - 0,95) \leq 0,56$
DLF_2	$0,054 + 0,0088 \cdot f_s$	$0,069 + 0,0112 \cdot f_s$
DLF_3	$0,026 + 0,015 \cdot f_s$	$0,033 + 0,0192 \cdot f_s$
DLF_4	$0,010 + 0,0204 \cdot f_s$	$0,013 + 0,026 \cdot f_s$

$$DLF_1 = 0,0115 f_s^2 + 0,2803 f_s - 0,2902$$

$$DLF_2 = 0,0669 f_s^2 + 0,1067 f_s - 0,0417$$

$$DLF_3 = 0,0247 f_s^2 + 0,1149 f_s - 0,1518$$

$$DLF_4 = -0,0039 f_s^2 + 0,0285 f_s - 0,0082$$

$$\varphi_1 = 0$$

$$\varphi_2 = \frac{\pi}{180} \cdot (-99,76 f_s^2 + 478,92 f_s - 387,8)$$

$$\varphi_3 = \frac{\pi}{180} \cdot (-150,88 f_s^3 + 819,65 f_s^2 - 1431,35 f_s$$

$$+ 811,93), \quad \text{for } f_s < 2 \text{ Hz}$$

$$\varphi_3 = \frac{\pi}{180} \cdot (813,12 f_s^3 - 5357,6 f_s^2 + 11726 f_s - 8505,9),$$

for $f_s \geq 2 \text{ Hz}$

$$\varphi_4 = \frac{\pi}{180} \cdot (34,19 \cdot f_s - 65,14)$$

(22)

The Fourier series resulting by using the presented load parameters from [4–8,49], are shown in Fig. 11 exemplarily with the step frequency of $f_s = 2.0 \text{ Hz}$. As for the gait parameters, the literature offer a large variety of different information for the load parameters. This can be explained by the different human walking patterns, which means that even two pedestrians with the same weight and the same step frequency can still walk differently and thus, induce different load amplitudes in the structure. In order to account for the uncertainty in the Fourier series, the Fourier parameters are modeled with fuzzy variables. For every Fourier parameter, a minimum value $DLF_{i,\min}$, $\varphi_{i,\min}$, a maximum value $DLF_{i,\max}$, $\varphi_{i,\max}$ and a mean value $DLF_{i,\text{mean}}$, $\varphi_{i,\text{mean}}$ is chosen based on the parameters from the six presented Fourier series in Fig. 11. The limit values are assigned to the membership $\mu = 0$ and the mean value is assigned to the membership $\mu = 1$. Therefore, triangular membership functions are defined for the Fourier parameters

$$\widetilde{DLF}_i = \langle DLF_{i,\min} \quad DLF_{i,\text{mean}} \quad DLF_{i,\max} \rangle \quad (23)$$

$$\widetilde{\varphi}_i = \langle \varphi_{i,\min} \quad \varphi_{i,\text{mean}} \quad \varphi_{i,\max} \rangle$$

In this paper, the modeled Fourier series using fuzzy variables is referred to as fuzzy Fourier series (FFS). The fuzzy Fourier coefficients and fuzzy phase shifts are referred to as fuzzy Fourier parameters (FFP). In order to choose appropriate fuzzy variables, the five dynamic load factors DLF_i and four phase shifts φ_i taken from literature are represented in Fig. 12. The fifth phase shift is given as $\varphi_5 = 0$ for all

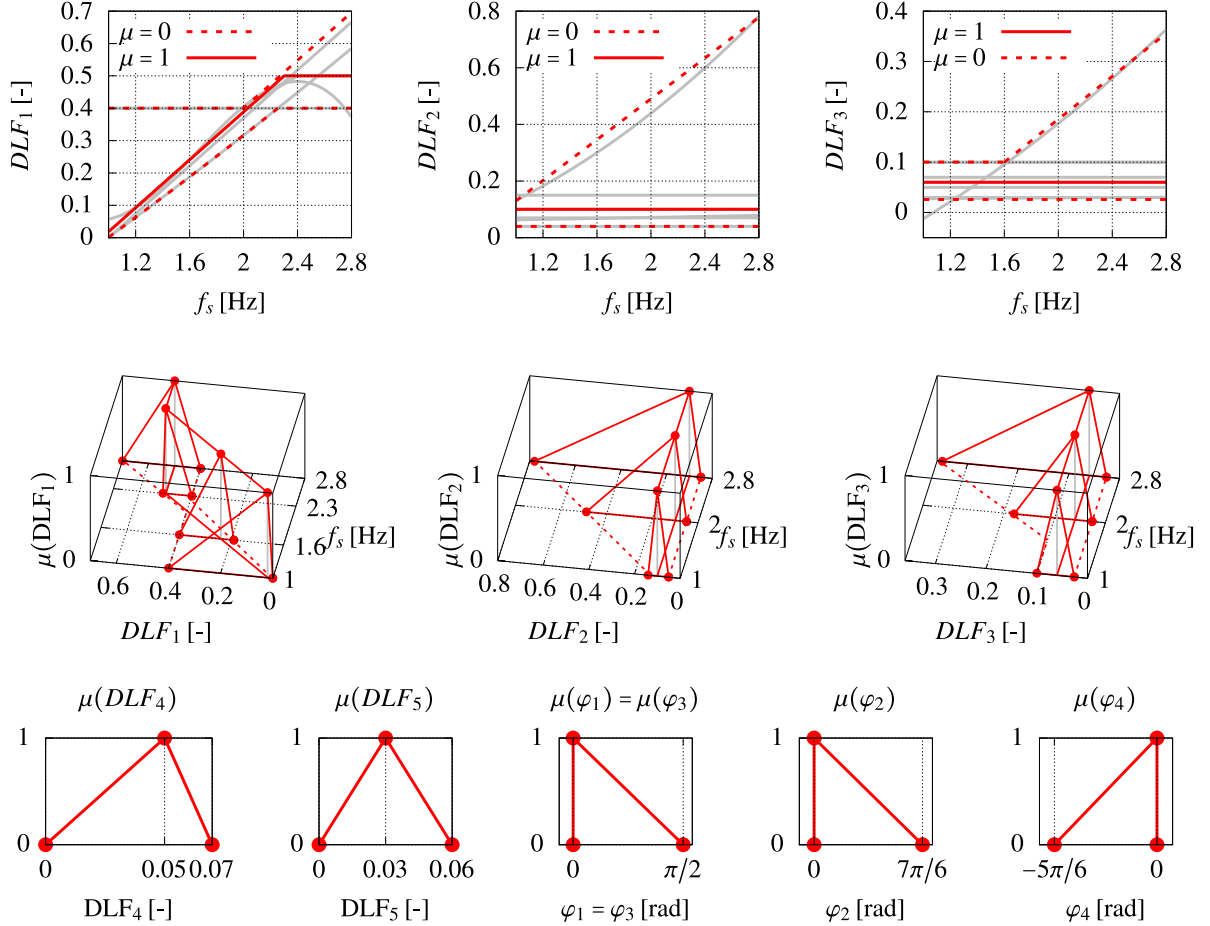


Fig. 13. Fuzzy variables for the Fourier parameters: twodimensional (top) and threedimensional (middle) representation of the fuzzy functions for the first three dynamic load factors, fuzzy numbers for the fourth and fifth dynamic load factor and the phase shifts (bottom).

of the six mentioned authors and therefore is not considered for the uncertainty quantification.

The results from Young [4] are presented as 50%-exceedance probability, also called median. The results from Kerr [6] are represented as continuous lines for $E[DLF_i]$ and dashed lines for $E[DLF_i] \pm \sigma_{DLF_i}$. As the Fourier series is a sum of 2π -periodical functions, there is no difference between the phase shift φ_i and $\varphi_i + 2n\pi$ if n is an integer. Therefore, the value for φ_2 according to Seiler&Hüttner [7], which is given as $\varphi_2 = -5\pi/6$, is visualized in Fig. 12 as $\varphi_2 = -5\pi/6 + 2\pi = 7\pi/6$. The reason of this representation is to better find an appropriate fuzzy variable, because the value $7\pi/6$ is closer to the values of the other authors. The first three dynamic load factors DLF_1 , DLF_2 and DLF_3 have functional dependencies from the step frequency f_s and therefore are defined as fuzzy functions according to Eqs. (23), (24), (25) and (26).

$$DLF_{1,\min} = \begin{cases} 0.324 \cdot f_s - 0.3224, & f_s < 2.22 \text{ Hz} \\ 0.4, & f_s \geq 2.22 \text{ Hz} \end{cases}$$

$$DLF_{1,\text{mean}} = \begin{cases} 0.37 \cdot (f_s - 0.95), & f_s < 2.3 \text{ Hz} \\ 0.5, & f_s \geq 2.3 \text{ Hz} \end{cases} \quad (24)$$

$$DLF_{1,\max} = \begin{cases} 0.4, & f_s < 2.0 \text{ Hz} \\ 0.37 \cdot f_s - 0.34, & f_s \geq 2.0 \text{ Hz} \end{cases}$$

$$DLF_{2,\min} = 0.05$$

$$DLF_{2,\text{mean}} = 0.1$$

$$DLF_{2,\max} = 0.36 \cdot f_s - 0.23 \quad (25)$$

$$DLF_{3,\min} = 0.025$$

$$DLF_{3,\text{mean}} = 0.06$$

$$DLF_{3,\max} = \begin{cases} 0.1, & f_s < 1.6 \text{ Hz} \\ 0.22 \cdot f_s - 0.26, & f_s \geq 2.0 \text{ Hz} \end{cases} \quad (26)$$

For the second and third DLF, the minimum and the mean value are constant, while the maximum value is a function of f_s . The fuzzy functions assign every pedestrian with his own step frequency f_s , to a corresponding fuzzy triangular number. In this way, every pedestrian has an individual fuzzy number for the first three dynamic load factors. The fourth and the fifth dynamic load factors DLF_4 and DLF_5 as well as the phase shifts φ_i have constant limits and are therefore modeled with fuzzy numbers

$$\widetilde{DLF}_4 = \langle 0 \ 0.05 \ 0.07 \rangle, \quad \widetilde{DLF}_5 = \langle 0 \ 0.03 \ 0.06 \rangle,$$

$$\tilde{\varphi}_1 = \tilde{\varphi}_3 = \langle 0 \ 0 \ \pi/2 \rangle, \quad \tilde{\varphi}_2 = \langle 0 \ 0 \ 7\pi/6 \rangle,$$

$$\tilde{\varphi}_4 = \langle -5\pi/6 \ 0 \ 0 \rangle. \quad (27)$$

The first and third phase shift φ_1 , φ_3 is modeled with the same fuzzy variable $\tilde{\varphi}_1 = \tilde{\varphi}_3$. The fuzzy functions for the first three dynamic load factors are represented two-dimensionally in Fig. 13 (top) and three-dimensionally in Fig. 13 (middle). The triangular fuzzy numbers are visualized in Fig. 13 (bottom).

The fuzzy Fourier series (FFS) has the objective to account for the Fourier series from six different authors in one model. Together with the fp-r-variable for the step frequency f_s presented in Section 4.1 and the nine fuzzy Fourier variables, every pedestrian is modeled with

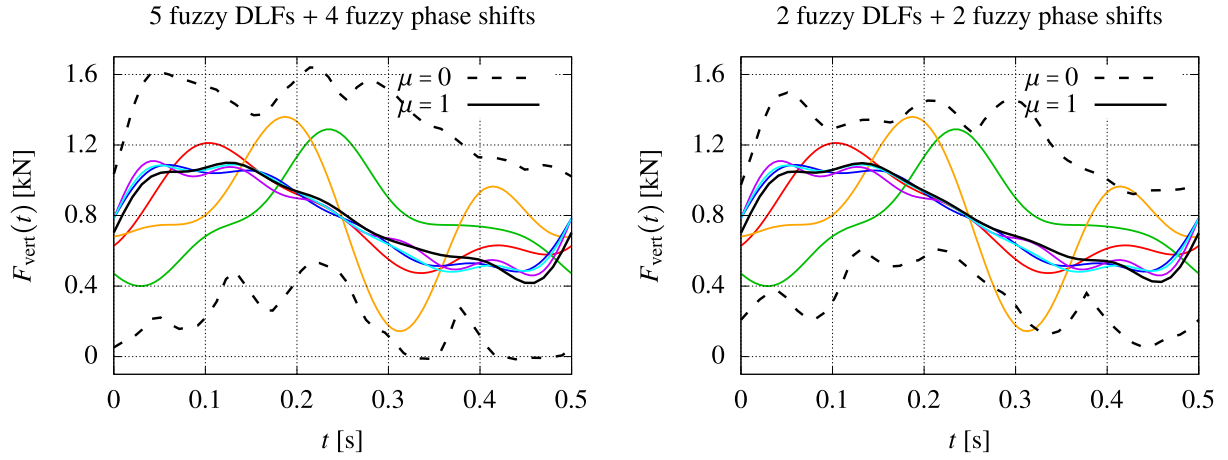


Fig. 14. Fuzzy process of the Fourier series with $f_s = 2.0$ Hz: with all nine FFPs (left) and with only the first two fuzzy DLFs and fuzzy phase shifts (right).

eleven fuzzy variables. This amount of input variables results in an immense computational cost. Moreover, possible dependencies (correlations) between the fuzzy input variables can lead to an overestimated fuzzy load process $\tilde{F}_{\text{vert}}(t)$. At this point, the question arises whether all fuzzy variables are necessary to obtain a realistic result. If some of the fuzzy variables do not provide any sensitivity on the output, they can be replaced with deterministic variables in order to reduce the computational effort. The aim is to find the lowest number of fuzzy variables to best account for the six different Fourier series. Therefore, the FFS with all nine FFPs is compared with the FFS with only the first two fuzzy DLFs and fuzzy phase shifts (four FFPs), see Fig. 14. Obviously, the FFS with all nine FFPs has clearly larger support bounds ($\mu = 0$) compared with 4 FFPs. However, the six Fourier series are almost completely contained in the support bounds of the FFS with four FFPs. This shows, that four FFPs are sufficient, in order to consider the uncertainty of the Fourier series for walking pedestrians. The remaining parameters, up to the fifth harmonic, are modeled as deterministic variables.

5. Numerical examples

In this section, the results of the fuzzy-stochastic analysis are presented in two examples. The first example is a simply supported single-span beam as simplified static system of a footbridge. The second example is a 3D-model of a real world footbridge. Random groups of pedestrians walking over the bridge are modeled with the uncertainty models introduced in Section 4. The resulting structural accelerations are calculated with the three-loop computational model explained in Section 3. The surrogate models used in this paper are calculated with the HDMR method with LSQ polynomials. The α -level optimization (ALO) is realized with the particle swarm optimization algorithm. The structural accelerations should not exceed a specific limit value, to ensure the pedestrians comfort. Therefore, the stochastic parameter of interest is chosen as the 95%-quantile value. The output of the fuzzy-stochastic-analysis is the fuzzy 95%-quantile value of the maximum structural acceleration. In the second example, the comfort level of the footbridge is assessed by recommendations from the guideline DIN EN 1990 [58] and uncertainty models are defined for the material parameters (stiffness, density, damping ratio).

5.1. Single span beam

The first example is a single span reinforced concrete beam with a span length of $L = 25$ m, one simple and one pinned support. The cross-section is a T-beam with the geometrical parameters presented in Fig. 16. The web heights h_w used in this example is a design parameter with $h_w = 0.4$ m, $h_w = 0.5$ m, $h_w = 0.6$ m and $h_w = 0.7$ m. The

Table 7

First two structural eigenfrequencies and Rayleigh-damping parameters with respect to the different web heights.

h_w [m]	f_1 [Hz]	f_2 [Hz]	α [s^{-1}]	β [s]
0.4	1.74	6.96	0.2273	$4.7587 \cdot 10^{-4}$
0.5	2.03	8.12	0.2655	$4.0744 \cdot 10^{-4}$
0.6	2.34	9.36	0.3053	$3.5427 \cdot 10^{-4}$
0.7	2.65	10.6	0.3462	$3.1246 \cdot 10^{-4}$

material parameters are: Young's modulus $E = 34000$ MN/m², mass density $\rho = 2500$ kg/m³ and damping ratio $\xi = 0.013$ [–]. The FE-model consists of 10 Bernoulli beam elements and the load is a group of 15 pedestrians walking over the bridge. The time delay Δt between two consecutive pedestrians is calculated as random variable according to Eqs. (18) and (19). The time integration is computed with the implicit Newmark method [37] with the time increment $dt = 0.01$ s and the standard Newmark-parameters $\gamma = 0.5$ and $\beta = 0.25$. The simulation time T [s] is the time needed by the entire pedestrian group to cross the bridge and depends on the pedestrians walking speeds, which are variable. Therefore, the simulation time is recalculated as variable in every simulation. The structural eigenfrequencies f_i and angular eigenfrequencies ω_i can be calculated with the analytical solution for simply supported single span beams

$$f_i = \frac{i^2 \pi}{2} \sqrt{\frac{EI}{\rho AL^4}} \quad , \quad \omega_i = 2\pi f_i \quad . \quad (28)$$

The Rayleigh-damping parameters α and β are calculated with the damping ratio ξ and the first two angular eigenfrequencies ω_1 and ω_2

$$\alpha = 2\xi \frac{\omega_1 \omega_2}{\omega_1 + \omega_2} \quad , \quad \beta = 2\xi \frac{1}{\omega_1 + \omega_2} \quad . \quad (29)$$

The first structural eigenfrequencies and the Rayleigh-damping parameters with respect to the different web heights h_w are presented in Table 7.

Every modeled pedestrian crosses the bridge with the coordinate $x(t)$ and the load vector $\mathbf{F}(t)$ and has uncertain characteristics like step frequency f_s , velocity $v = \dot{x}(t)$ and body weight G . Two random pedestrians walking over the beam with the load $F_i(t)$ at the position $x_i(t)$ are represented in Fig. 15. The step frequency of the pedestrians is modeled with the fp-r variable presented in Section 4.1 and the Fourier series for the load is calculated with the load parameters presented in Section 4.2. The surrogate model is generated with the HDMR method of 2nd order based on the LSQ polynomial approximation of the 5th degree and a number of $n_{\text{sim}} = 7$ sample points per dimension with equidistant sampling. At first, the surrogate models are calculated using the six Fourier series from Section 4.2 and the fp-r variable for the step frequency f_s , see Fig. 17. For the first three web heights of $h_w = 0.4$ m,

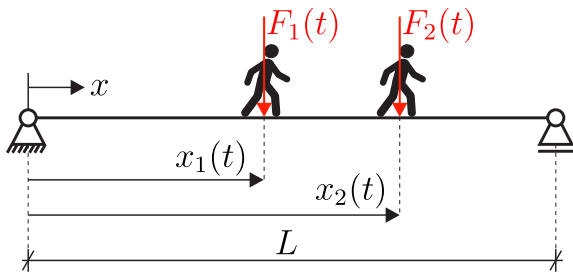


Fig. 15. Two pedestrians walking with the vertical loads $F_i(t)$ at the coordinate $x_i(t)$ on a footbridge with the span length L , which is simplified as a simply supported single-span beam.

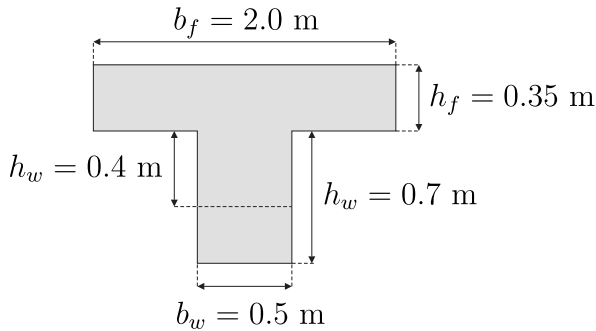


Fig. 16. T-beam with flange width b_f , flange height h_f , web width b_w and web heights h_w from $h_w = 0.4$ m to $h_w = 0.7$ m.

$h_w = 0.5$ m and $h_w = 0.6$ m, the first structural eigenfrequencies f_1 are in the range of the fuzzy mean value of the step frequency $\tilde{E}[f_s]$, which leads to strong resonance effects. This is visible in the surrogate models, where the global maximum is located at $E[f_s] = f_1$ and the smallest standard deviation $\sigma_{f_s} = 0.08$ Hz. For the fourth web height of $h_w = 0.7$ m, the structural eigenfrequency is out of the range of $\tilde{E}[f_s]$. This means that the strongest resonance is achieved with the highest mean value and standard deviation, which is also visible in the global maximum of the surrogate model of $h_w = 0.7$ m. This confirms the importance of resonance effects and shows, that the choice of an appropriate variable for the step frequency has a relevant influence on the structural accelerations.

The α -Level optimization yields the fuzzy CDF of the maximum acceleration. As an example, the fuzzy CDF for the maximum acceleration for a web height of $h = 0.7$ m is represented in Fig. 18. In this figure it is shown, how the output variable, which is the fuzzy 95%-quantile, is extracted from the fuzzy CDF at the coordinate $F(a_{\max}) = 0.95$. This output variable is compared with the output from the FFS with four FFPs and with nine FFPs in Fig. 19. The output obtained by the six Fourier series, represented in different colors in Fig. 19 (left), are considered as reference solution for the FFS. This means, that the fuzzy output obtained by the FFS, should approximate the union of the fuzzy outputs obtained by the six Fourier series. With two inputs for the fuzzy variable of the step frequency f_s and nine fuzzy variables for the fuzzy-Fourier series (FFS), the total number of fuzzy input variables is $M = 11$. With that, the total number of sample points N_{sim} is calculated to $N_{\text{sim}} = 2047$ with Eq. (15). The MCS is realized with 5000 samples on every of the 2047 sample points, leading to a total of $2047 \cdot 5000 = 10235000$ realizations of the deterministic solution. With four FFPs and a total of $M = 6$ fuzzy input variables, the total number of sample points reduces to $N_{\text{sim}} = 577$, which is a reduction factor of approximately 3.55. In this example, both the fuzzy outputs and the surrogate models obtained by the six Fourier series are very similar in size and shape. Only for $h_w = 0.4$ m, the six results are quite different. In particular, the result obtained by the Fourier series according to

Table 8

Comfort levels for vertical acceleration according to [58].

Comfort levels	$a_{\text{lim,vertical}}$ [m/s ²]	Perceived vibrations
CL3	≤ 0.5	Not noticeable
CL2	≤ 1.0	Slightly noticeable
CL1	≤ 2.5	Strongly noticeable
CL0	> 2.5	Not acceptable

SYNPEX is the only one with a distinctive form, that sets it apart from the others. This shows, that the uncertainty in the Fourier series can be revealed more or less noticeable in the results, depending on the analyzed structure.

The results show, that the two FFS versions (4 FFPs and 9 FFPs) are about the same on the highest α -level ($\mu = 1$). However, the right bound of the outputs with nine FFPs, especially in the examples with $h_w = 0.5$ m and $h_w = 0.6$ m, clearly exceed the reference solutions on the bottom alpha-level, while the outputs with four FFPs are closer to the reference solutions. Considering both the left and right bounds, the outputs with nine FFPs are much wider than the reference solution in comparison to those with four FFPs. It is clear, that more fuzzy input variables lead to a wider output. The results show that the FFS with nine FFPs is not appropriate to realistically replace the six Fourier series. In summary, the version with four FFPs, not only reduces the computational effort significantly, but also leads to a better approximation of the six Fourier series, compared to the version with all nine FFPs. Therefore, the usage of the version with all nine FFPs is not recommended.

For the assessment of vibrations in the limit state of serviceability, the standard DIN EN 1990 [58] suggests comfort levels (CL) defined by limit values for the structural accelerations, given in Table 8. Because the output variable is fuzzy, it can belong to more than one CL. In order to assess the structure within CLs, the output membership function can be divided in partial areas using the comfort limits.

The partial areas in the CLs are colored green (CL3), yellow (CL2) and red (CL1). The output with four FFPs and the web heights of $h_w = 0.4$ m and $h_w = 0.7$ m are divided in CLs in Fig. 20. Another possible assessment method is the centroid of the membership function, also shown in Fig. 20. This is referred to as “defuzzification” because it reduces the fuzzy output to a deterministic value. This can be useful when comparing the quantity of interest with other deterministic values such as, e.g., the comfort limits. It is also possible to combine both assessment methods, considering the centroid and the partial areas. A possible request in footbridge design could be the elimination of the red area (CL1) and the centroid to be in the green area (CL3). In this case, the web height of $h_w = 0.4$ m is not satisfying, as the centroid is in the yellow area (CL2) and there is a notable red area (CL1). A satisfying solution would be the web height of $h_w = 0.7$ m as there is no red area and the centroid is in the green area (CL3). In the described scenario, the bridge with the web height of $h_w = 0.7$ m represents the optimal solution out of the four presented examples. In general, massive structures are more resistant to vibrations, but at the same time are more expensive in material. Therefore, the optimization of a specific design parameter (e.g. web height h_w) while considering the objective of material savings, is an optimization-problem with contrary goals. In order to systematically find the optimal structure, the presented model could be improved in future works, through the implementation of an optimization algorithm with polymorphic uncertainty.

5.2. 3D-model of a real footbridge

The second example is a 3D FE-model of a real-world bridge, located in Wurmberg (Germany), see Fig. 21. The bridge has a total span length of $L = 50$ m and a cross-section width of $b = 2.5$ m. The cross-section height h is variable over the longitudinal axis because the bridge is

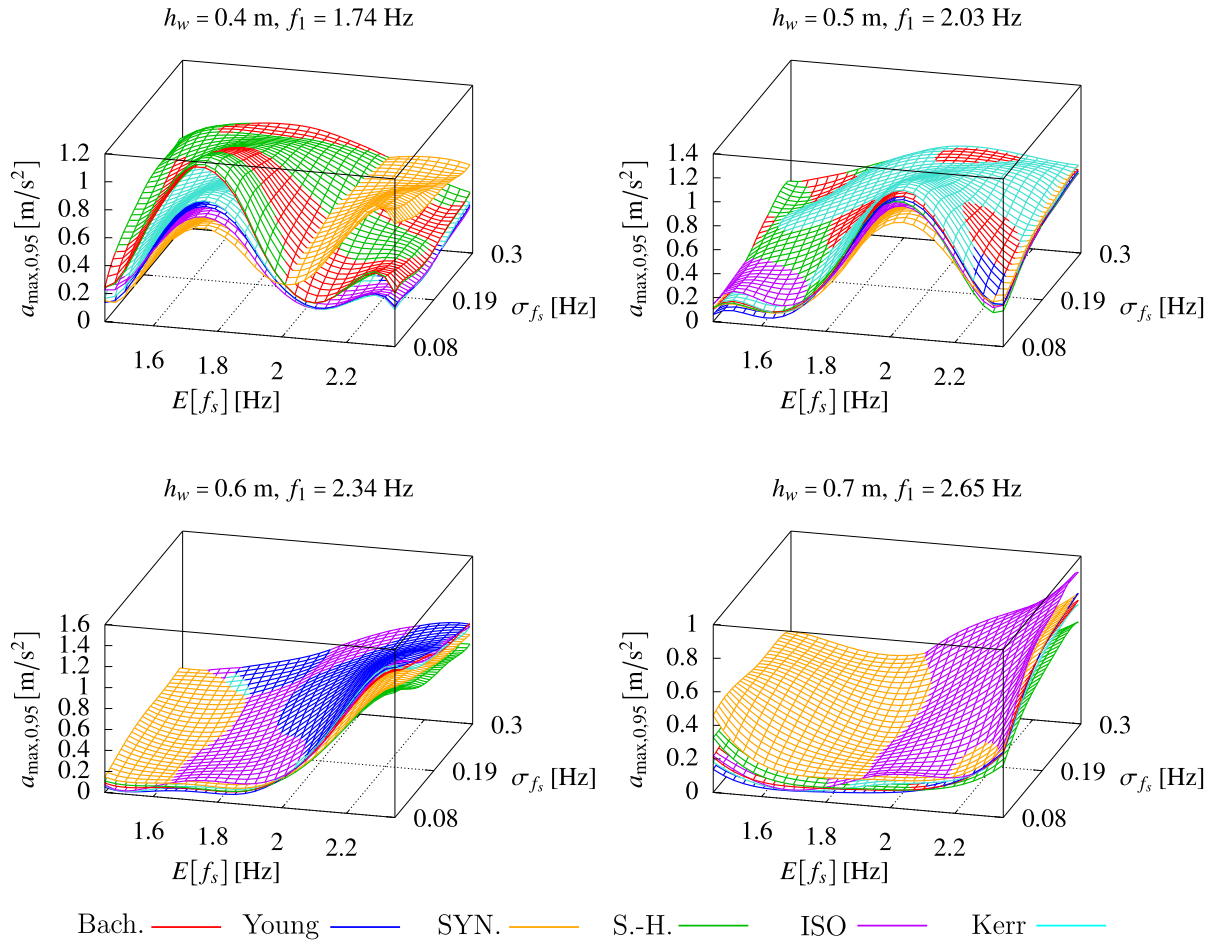


Fig. 17. Surrogate models obtained by the six Fourier series with four different web heights $h_w = 0.4 - 0.7$ m.

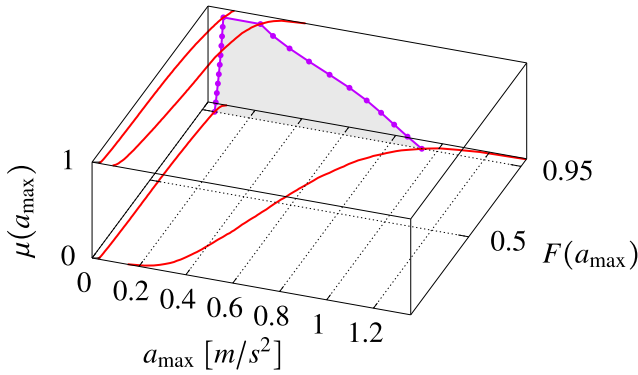


Fig. 18. Fuzzy CDF with cutting surface at $F = 0.95$ for the maximal acceleration of the beam with a web height of $h = 0.7$ m with the Fourier series according to ISO 10137 [8].

curved with the radius of curvature of $R = 250$ m and the opening angle of $\theta = 5.74^\circ$. The maximum height is located in the middle of the bridge with $h_{\max} = 2.20$ m and the minimum height is located at the edges with $h_{\min} = 0.667$ m. The bridge is made of a slightly curved concrete shell with a thickness of $t = 0.20$ m and a width of $b = 2.5$ m. The underlying steel structure is made of round and hollow beams, divided into longitudinal and diagonal beams. The three longitudinal beams, one larger main beam and two upper beams, extend across the entire span length. The diagonal beams are connected with the upper longitudinal beams at the distance of 0.71 m from the axis of symmetry

and with the underlying main beam in a “V-shape”. The connections are designed as rigid in bending with welded joints. The main beam has a diameter of $D_1 = 0.367$ m and a thickness of $t_1 = 0.039$ m. The two upper beams have the same cross-sectional dimensions as the diagonal beams: $D_2 = 0.2$ m and $t_2 = 0.02$ m. The typical material parameters for the Young’s modulus E and the density ρ of concrete and steel and the damping ratio ξ for composites are: $E_c = 34000$ [MN/m²], $\rho_c = 2.5$ [t/m³], $E_s = 210000$ [MN/m²], $\rho_s = 7.85$ [t/m³] and $\xi = 0.006$ [–].

The bridge is modeled in FEAP [36], using shell elements for the superstructure and Bernoulli beam elements for the beams. The FE-model is represented in Fig. 22 and consists of 1119 nodes and 914 elements. The geometrical information is shown in Fig. 23. The cross section in the middle of the bridge is represented in Fig. 24. For the numerical implementation of the pedestrian-induced loads, the bridge surface is discretized into three lanes along which the pedestrians can walk: the centerline and two sidelines 0.71 m away from the centerline. The lane can be chosen randomly for each pedestrian, which is accomplished with a uniformly distributed random variable that can take on natural numbers from one to three: $n_{\text{lane}} \in \{1, 2, 3\}$. The discretization of the bridge surface is shown in Fig. 25 in top view. In order to produce significant structural accelerations, the pedestrian group consists of 40 persons. The time integration is computed with the implicit Newmark method [37] analogous to the previous example. The time step is $dt = 0.1$ s, the simulation time of one bridge crossing is $T = 120$ s and the time delay Δt between two consecutive pedestrians is calculated with Eqs. (18) and (19). The numerical implementation with FEAP requires the specification of the node, of which the vertical acceleration amplitude is observed. The highest acceleration is often located in the middle of the bridge, but not necessarily. In order to

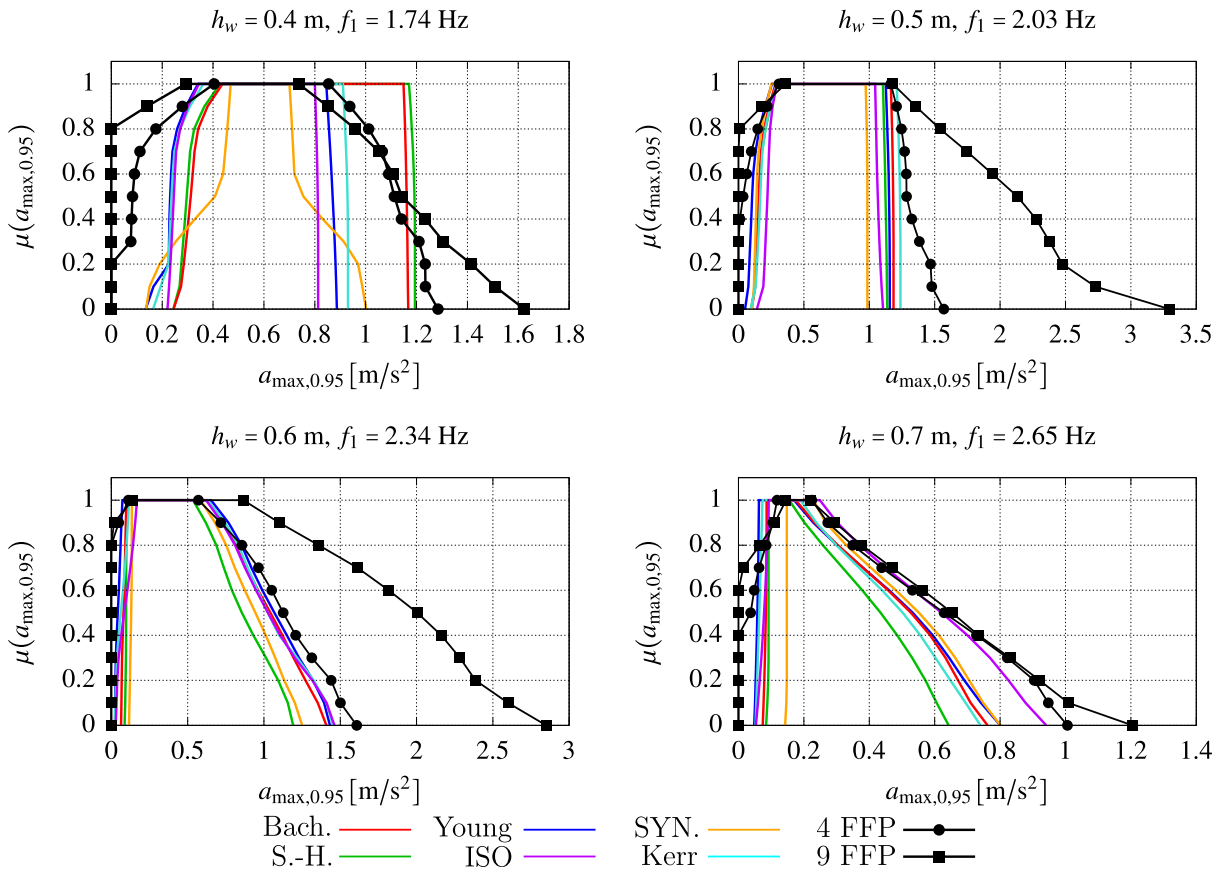


Fig. 19. Fuzzy outputs obtained by the six Fourier series with four different web heights $h_w = 0.4 - 0.7$ m. Comparison with 4 FFPs and 9 FFPs.

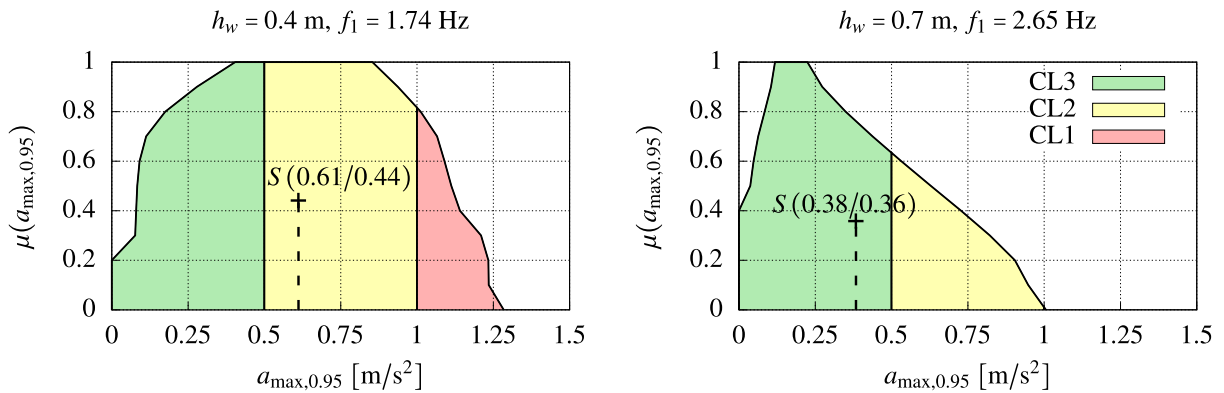


Fig. 20. Comfort assessment of the fuzzy outputs with four FFPs for the web height $h_w = 0.4$ m (left) and $h_w = 0.7$ m (right). (For interpretation of the references to color in this figure legend, the reader is referred to the web version of this article.)



Fig. 21. Footbridge across the Autobahn A8 at Wurmberg (BW, Germany).

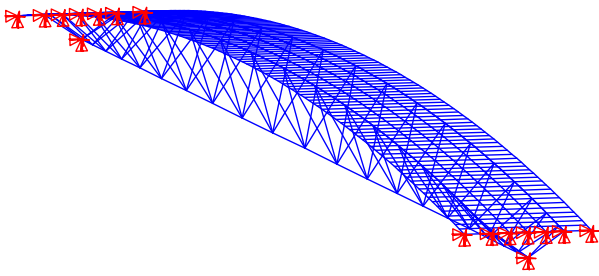


Fig. 22. FE-model of the footbridge, perspective view.

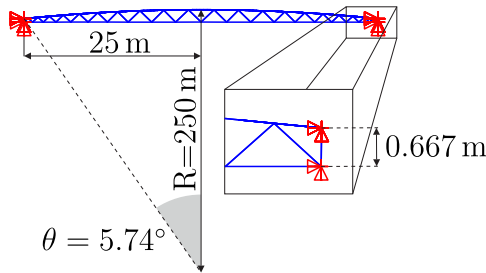


Fig. 23. Geometric parameters, side view.

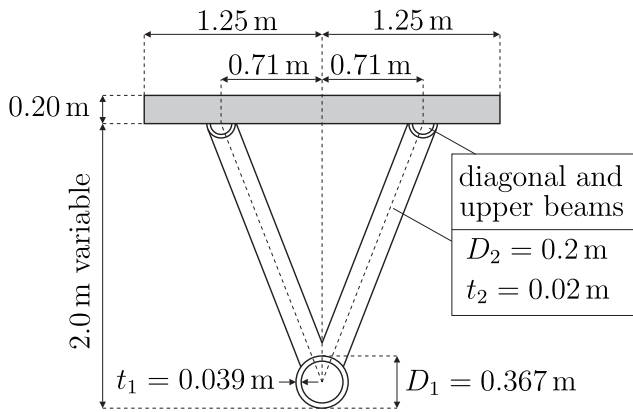


Fig. 24. Representation and dimensions of the average cross-section.

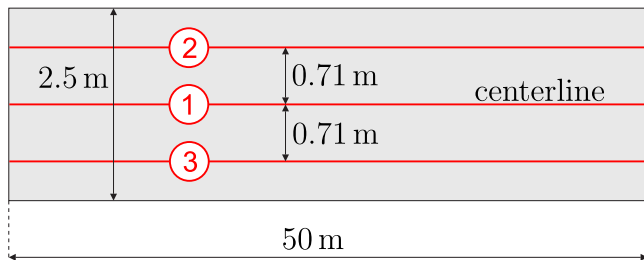


Fig. 25. Walking lanes discretization on the bridge surface, top view.

make a reasonable assumption about the location of the node with the highest acceleration amplitude, the first three eigenmodes of the bridge are taken into consideration. They are shown together with the respective eigenfrequencies in Fig. 26. The first eigenmode is vertical with $f_1 = 2.98$ Hz, the second eigenmode is lateral with $f_2 = 3.17$ Hz and the third eigenmode is torsional with $f_3 = 5.84$. Considering the torsional mode, the highest vertical acceleration amplitude of the bridge is supposed to be located in the middle of the bridge at the outer edge.

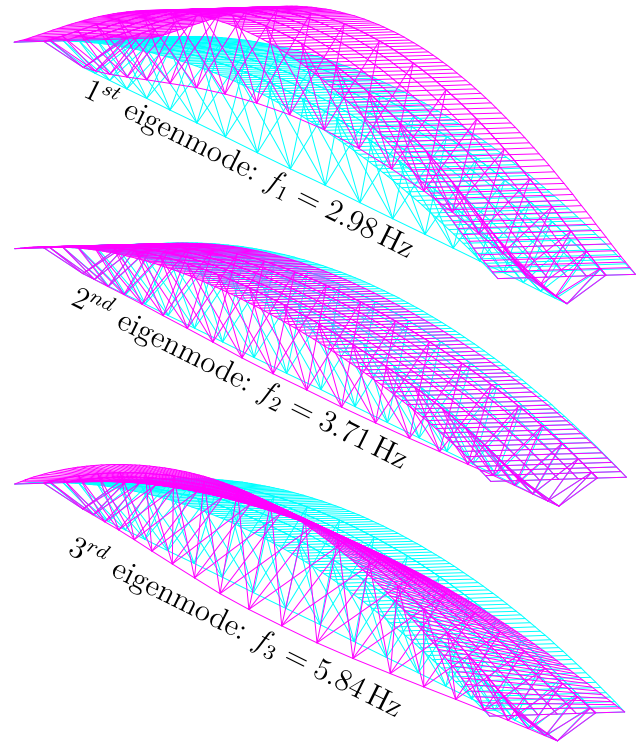


Fig. 26. Perspective view of the first three eigenmodes.

The uncertainty model for human-induced vibrations presented so far, considers the uncertainties in the parameters of walking pedestrians. The step frequency f_s is modeled with the same fp-r variable as in the previous examples. Because of the high computational effort, the FFS is modeled with only the first DLF as fuzzy function, while the remaining FFPs are deterministic variables. For the real-world footbridge, uncertainty models for material parameters are added to the previous model. Therefore, the Young's modulus E and the mass-density ρ of concrete and steel are modeled as a normal distributed random variables, with the following mean values: $E[E_c] = 34000$ MN/m², $E[E_s] = 210000$ MN/m², $E[\rho_c] = 2.5$ t/m³, $E[\rho_s] = 7.85$ t/m³. The standard deviations are 10% of the mean values in the case of the stiffness and 5% in the case of the mass-density, according to [59]. For comfort assessments of vibrating footbridges in the limit state of serviceability, the guideline SYNPEX [5] recommends minimum and average values for damping ratios ξ according to construction materials. In the case of a steel-concrete composite structure, the recommendations are $\xi_{\min} = 0.3\%$ and $\xi_{\text{average}} = 0.6\%$. Based on this information, here, the damping ratio ξ is modeled with the following right triangle as fuzzy variable: $\tilde{\xi} = \langle 0.003 \ 0.006 \ 0.006 \rangle$. The uncertain variables used in this example are summarized in Table 9. The Rayleigh-damping parameters α and β are calculated in each simulation with respect to the material parameters.

The surrogate model is generated with the LSQ method of the 3rd degree and $n_{\text{sim}} = 5$ sample points per dimension with equidistant sampling. With two inputs for the fp-r variable and one input for the first DLF of the FFS, the total number of sample points is $N_{\text{sim}} = 127$. With 200 MCS samples on every of the 127 sample points, this leads to a total of $127 \cdot 200 = 25400$ realizations of the dynamic structural analysis. The HDMR method of second order is used to view the cut function for $a_{\text{max},0.95}(E[f_s], \sigma_{f_s})$ [m/s²], which is represented in Fig. 27 with a discretization grid of 30 evaluation points per dimension. The global maximum is at the edge $a_{\text{max},0.95}(E[f_s] = 2.35, \sigma_{f_s} = 0.08) = 1.24$ m/s², because it has the highest probability to hit the first eigenfrequency $f_1 = 2.98$ Hz. The comparison between the two fuzzy outputs, by using

Table 9
Polymorphic uncertainty quantification of the variables used for the pedestrians and the footbridge.

Parameter	Uncertainty model	Variable
Step frequency f_s	fp-r variable	$\tilde{E}[f_s] = \langle 1.45 \ 1.70 \ 2.05 \ 2.35 \rangle$, $\tilde{\sigma}_{f_s} = \langle 0.08 \ 0.11 \ 0.19 \ 0.3 \rangle$
DLF_1	Fuzzy function	$\tilde{DLF}_1(f_s) = \langle DLF_{1,\min} \ DLF_{1,\text{mean}} \ DLF_{1,\max} \rangle$
Damping ratio	Fuzzy variable	$\tilde{\xi} = \langle 0.003 \ 0.006 \ 0.006 \rangle$
Material stiffness	Normal distributed	$E[E_c] = 34000 \text{ MN/m}^2$, $\sigma_{E_c} = 3400 \text{ MN/m}^2$
Material density	Random variables	$E[E_s] = 210000 \text{ MN/m}^2$, $\sigma_{E_s} = 21000 \text{ MN/m}^2$ $E[\rho_c] = 2.5 \text{ t/m}^3$, $\sigma_{\rho_c} = 0.25 \text{ t/m}^3$ $E[\rho_s] = 7.85 \text{ t/m}^3$, $\sigma_{\rho_s} = 0.785 \text{ t/m}^3$
Female body weight	Normal distributed	$E[G_w] = 67 \text{ kg}$, $\sigma_{G_w} = 10 \text{ kg}$
Male body weight	Random variables	$E[G_m] = 80 \text{ kg}$, $\sigma_{G_m} = 10 \text{ kg}$
Time delay between pedestrians	Poisson distributed	$\Delta t = -(1/\lambda) \cdot \ln(1-r)$ [s], $r \in [0, 1]$ is a uniformly distributed random variable
Walking lane	Random variable	$n_{\text{lane}} \in \{1, 2, 3\}$ uniformly distributed

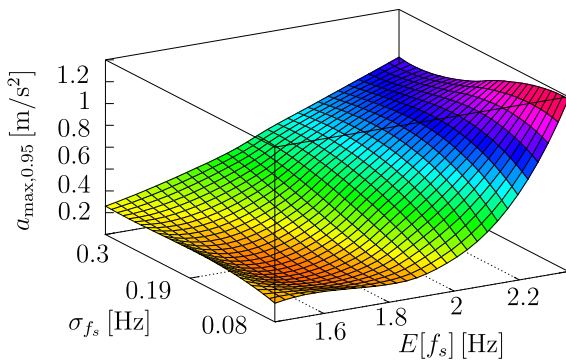


Fig. 27. HDMR 2nd order cut function for $a_{\max,0.95}(E[f_s], \sigma_{f_s})$ with the fuzzy Fourier series (FFS). (For interpretation of the references to color in this figure legend, the reader is referred to the web version of this article.)

a deterministic damping ratio $\xi = 0.006$ and the fuzzy damping ratio $\tilde{\xi} = \langle 0.003 \ 0.006 \ 0.006 \rangle$, is shown in Fig. 28. The membership function obtained by fuzzy damping is much wider on the right bound, resulting in a larger area in CL1. This example shows, that the consideration of the uncertainty of the damping ratio can have a significant influence on the structural accelerations. The damping behavior of a structure is a very complex physical phenomenon and thus cannot be reliably predicted in the structural design process. Therefore, the damping ratio is a good example whereby the usage of a fuzzy variable is an appropriate way to deal with the uncertainty in a structural parameter. In the context of a real footbridge design process, the desired CL has to be specified by the stakeholders. If, for example CL2 is desired, the red area in Fig. 28 has to be minimized. This can be achieved with structural measures, e.g. increasing the diameter of the steel-beams to increase the eigenfrequency to be out of the range for the step frequencies of walking pedestrians. The output obtained with a damping ratio of $\xi = 0.006$ has a relatively small membership area in CL1 (red), which can be considered as acceptable. Therefore, an increase in damping, such as the use of a tuned mass damper, is also an option to achieve the desired CL for the footbridge. The benefit of using fuzzy variables is, that the CLs can be assessed gradually instead of deterministically. The membership function states, that the footbridge can belong to different CLs with different grades of possibility, which is represented by the size of the area under the membership function. This opens up new and flexible possibilities for assessment methods in bridge design. An associated footbridge design process is illustrated in Fig. 29.

6. Conclusions

In this paper, the concept of polymorphic uncertainty modeling is presented on the simulation of human-induced vibrations for the design

Membership functions $\mu(a_{\max,0.95})$

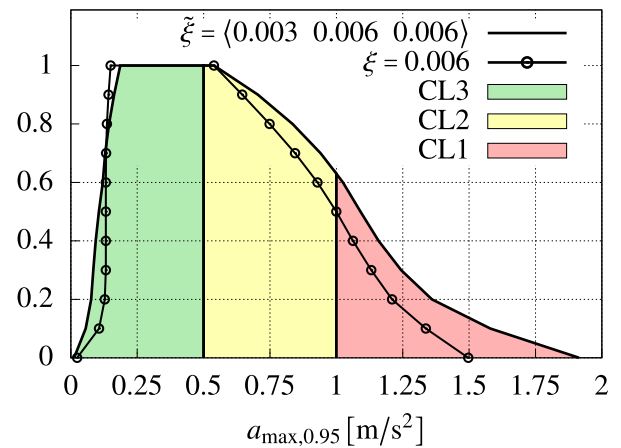


Fig. 28. Two fuzzy output variables: comparison between deterministic damping ratio ξ and fuzzy damping ratio $\tilde{\xi}$.

of footbridges. The approach focuses on the consideration of both the epistemic and aleatory uncertainties in the human load parameters, based on experimental data from literature sources. The step frequency f_s is modeled with two fuzzy variables: the fuzzy mean value $\tilde{E}[f_s]$ and the fuzzy standard deviation $\tilde{\sigma}_{f_s}$, leading to an fp-r variable. The dynamic load amplitude is described with the fuzzy Fourier series (FFS) with five harmonics. The results show that the uncertainty modeling of human load and structural parameters, has a significant influence on the output and thus, on the bridge assessment. The output variable, which is the fuzzy 95%-quantile value of the maximum structural acceleration, is classified within comfort levels (CL) from the design guideline. The bridge can belong to more than one CL with different grades of possibilities, which is defined by the membership function.

The comfort level is an indicator of how much the vibration is perceived by humans and at which acceleration they feel uncomfortable, which is very dependent of the individual. As every individual can have a different sensitivity to perceived vibrations, the comfort level could also be modeled as a fuzzy variable in future works. The desired CL of the footbridge and the aim of material savings are contrary objectives, because higher CL needs more material for a more vibration resistant structure. Thus, the structural design of the bridge while achieving both objectives, is an optimization problem. The presented model can be further improved by implementing an optimization algorithm in future works. In order to achieve higher efficiency, the presented method could be extended with the probability density evolution method (PDEM), according to [29].

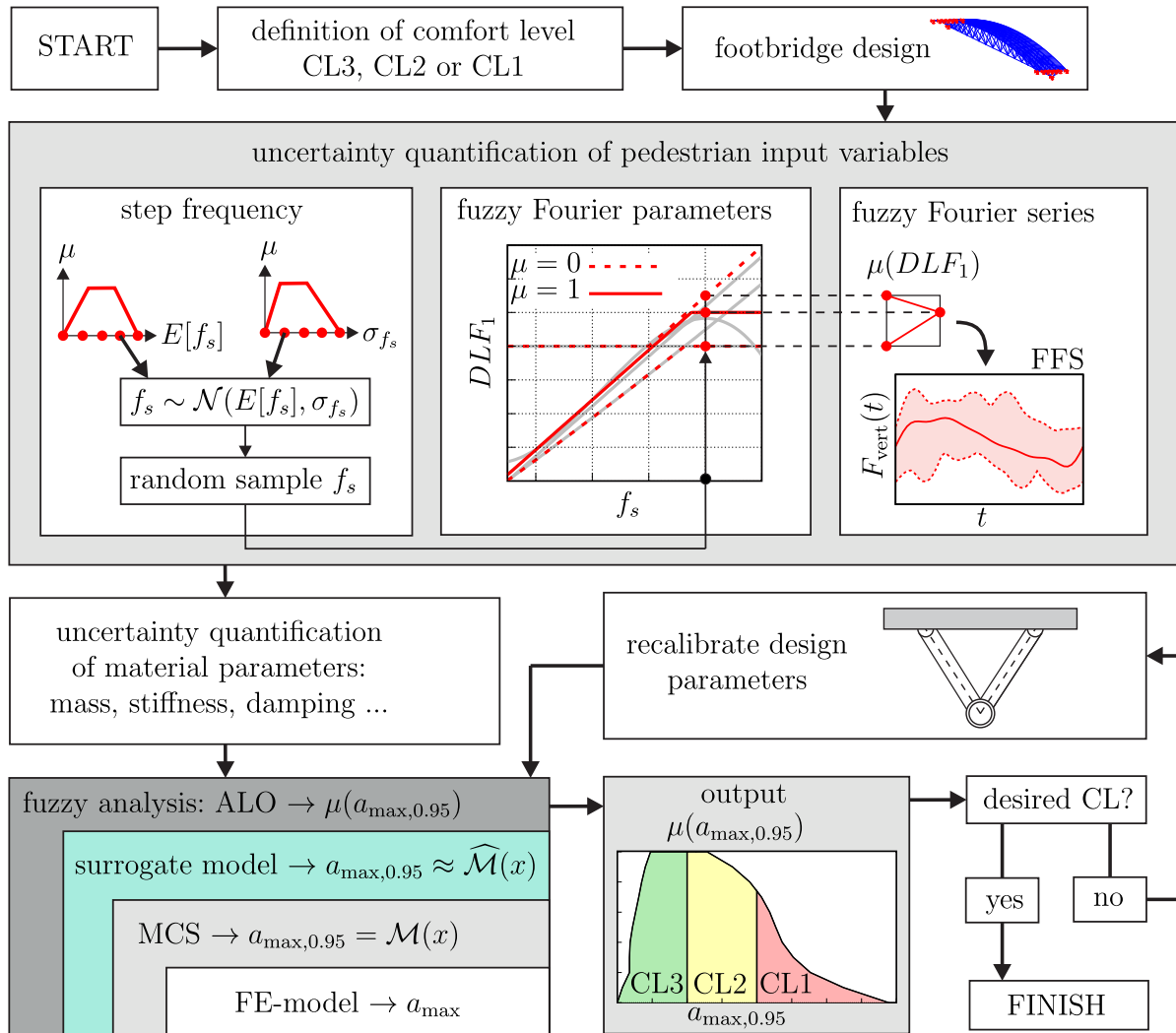


Fig. 29. Concept of the footbridge design process.

CRediT authorship contribution statement

Maximilian Schweizer: Conceptualization, Data curation, Formal analysis, Investigation, Methodology, Software, Validation, Visualization, Writing – original draft. **Marc Fina:** Conceptualization, Data curation, Funding acquisition, Methodology, Project administration, Resources, Software, Supervision, Validation, Writing – review & editing. **Werner Wagner:** Software, Writing – review & editing. **Slobodan Kasic:** Conceptualization, Writing – review & editing. **Steffen Freitag:** Writing – review & editing.

Declaration of competing interest

The authors declare that they have no known competing financial interests or personal relationships that could have appeared to influence the work reported in this paper.

Data availability

Data will be made available on request.

Acknowledgment

Financial support was provided by the Deutsche Forschungsgemeinschaft (DFG, German Research Foundation) in the framework of project 511267658. This support is gratefully acknowledged.

References

- [1] Dallard P, et al. The London MillenniumFootbridge. *Struct Eng* 2001;79(22):17–33.
- [2] Eurocode 1: Actions on structures - part 2: Traffic loads on bridges, EN 1991-2. European Committee for Standardisation (CEN); 2003.
- [3] Bachmann H, Ammann W. Vibration in structures - induced by man and machines. 1987, Structural Engineering Documents 3e, International Association of Bridge and Structural Engineering (IABSE), Zürich.
- [4] Young P. Improved floor vibration prediction methodologies. In: ARUP vibration seminar. 2001.
- [5] Feldmann M, Heinemeyer C, Butz C. In: Europäische Kommission, Generaldirektion Forschung und Innovation, editor. Advanced load models for synchronous pedestrian excitation and optimised design guidelines for steel footbridges (SYNPEX). Publications Office; 2009.
- [6] Kerr CS. Human induced loading on staircases [Ph.D. thesis], University of London, Mechanical Engineering Department; 1998.
- [7] Seiler C, Hüttner S. Ein einheitliches modell zur beschreibung von fußgängerlasten für verschiedene bewegungsarten - theorie, experimentelle messungen und praktische anwendung. *Bauingenieur* 2004;79:483–96.

- [8] International Organization for Standardization. ISO 10137: Bases for design of structures - serviceability of buildings and walkways against vibrations. 2007.
- [9] Atzwanger K, Schmitt A. Walking speed and depression: Are sad pedestrians slow? *Hum Ethol Bull* 1997;12.
- [10] Schmitt A, Atzwanger K. Walking fast-ranking high: A sociobiological perspective on pace. *Ethol Sociobiol* 1995;16(5):451–62.
- [11] Bornstein M. The pace of life: Revisited. *Int J Psychol* 1979;14(1–4):83–90.
- [12] Bornstein M, Bornstein H. The pace of life. *Nature* 1976;259(5544):557–9.
- [13] Wirtz P, Ries G. The pace of life - reanalysed: Why does walking speed of pedestrians correlate with city size? *Behaviour* 1992;123(1–2):77–83.
- [14] Moeller B, Beer M. Fuzzy randomness - uncertainty in civil engineering and computational mechanics. Springer-Verlag Berlin Heidelberg; 2004.
- [15] Möller B, Beer M. Engineering computation under uncertainty – capabilities of non-traditional models. *Comput Struct* 2008;86(10):1024–41.
- [16] Graf W, Götz M, Kaliske M. Structural design with polymorphic uncertainty models.. In: 6th International conference on reliable engineering computing. Chicago, 2014.
- [17] Edler P, Freitag S, Kremer K, Meschke G. Optimization approaches for the numerical design of structures under consideration of polymorphic uncertain data. *ASCE-ASME J Risk and Uncertain Eng Syst Part B* 2019;5(4):041013.
- [18] Schietzold FN, Graf W, Kaliske M. Multi-objective optimization of tree trunk axes in glulam beam design considering fuzzy probability-based random fields. *ASCE-ASME J Risk and Uncertain Eng Syst Part B* 2021;7(2):020913.
- [19] Fina M. Polymorphe Unschärfemodellierung in der nichtlinearen Strukturmechanik - Stabilität von Schalentragwerken, räumliche Variabilität und Metamodellierung [Dissertation], Institut für Baustatik, Karlsruher Institut für Technologie; 2020.
- [20] Fina M, Weber P, Wagner W. Polymorphic uncertainty modeling for the simulation of geometric imperfections in probabilistic design of cylindrical shells. *Struct Saf* 2020;82:101894.
- [21] Fina M, Wagner W, Graf W. On polymorphic uncertainty modeling in shell buckling. *Comput-Aided Civ Infrastruct Eng* 2023;38(18):2632–47.
- [22] Fina M, Panther L, Weber P, Wagner W. Shell buckling with polymorphic uncertain surface imperfections and sensitivity analysis. *ASCE-ASME J Risk Uncertain Eng Syst Part B* 2021;7(2):020909.
- [23] Weber P, Fina M, Wagner W. Time domain simulation of earthquake excited buildings using a fuzzy stochastic approach. In: Proceedings of the 29th European safety and reliability conference. Research Publishing Services; 2019.
- [24] Graf W, Götz M, Kaliske M. Analysis of dynamical processes under consideration of polymorphic uncertainty. *Struct Saf* 2015;52:194–201.
- [25] Zschocke S, Leichsenring F, Graf W, Kaliske M. A concept for data-driven computational mechanics in the presence of polymorphic uncertain properties. *Eng Struct* 2022;267:114672.
- [26] Schmidt A, Henning C, Herbrandt S, Könke C, Ickstadt K, Ricken T, et al. Numerical studies of earth structure assessment via the theory of porous media using fuzzy probability based random field material descriptions. *GAMM-Mitteilungen* 2019;42(1):e201900007.
- [27] Drieschner M, Petryna Y, Freitag S, Edler P, Schmidt A, Lahmer T. Decision making and design in structural engineering problems under polymorphic uncertainty. *Eng Struct* 2021;231:111649.
- [28] Chen J, Wang J, Brownjohn JMW. Power spectral-density model for pedestrian walking load. *J Struct Eng* 2019;145(2).
- [29] Ding G, Chen J. Influences of walking load randomness on vibration responses of long-span floors. *J Vib Eng* 2016;29:123–31.
- [30] Pancaldi F, Bassoli E, Milani M, Vincenzi L. A statistical approach for modeling individual vertical walking forces. *Appl Sci* 2021;11(21):10207.
- [31] Zivanovic S. Probability-based estimation of vibration for pedestrian structures due to walking [Dissertation], 2006.
- [32] Sahnaci C. Fakultät für Bau- und Umweltingenieurwissenschaften der Ruhr-Universität Bochum; 2013.
- [33] Brownjohn J, Pavic A, Omenzetter P. A spectral density approach for modelling continuous vertical forces on pedestrian structures due to walking. *Can J Civil Eng* 2004;31(1):65–77.
- [34] Kasperski M. Vibration serviceability for pedestrian bridges. *Struct Build* 2006;152:273–82.
- [35] Möller B, Graf W, Beer M. Fuzzy structural analysis using α -level optimization. *Comput Mech* 2000;26(6):547–65.
- [36] Taylor RL. FEAP. 2024, <http://www.ce.berkeley.edu/projects/feap/>.
- [37] Newmark NM. A method of computation for structural dynamics. *J Eng Mech Div* 1959;85(3):67–94.
- [38] Faes M, Fina M, Valdebenito M, Lauff C, Wagner W, Freitag S, et al. Bounding failure probabilities in imprecise stochastic FE models. In: Beer M, Zio E, Phoon K-K, Ayyub B, editors. Proceedings of the 8th international symposium on reliability engineering and risk management. 2022, Research Publishing.
- [39] Fina M, Faes M, Valdebenito M, Wagner W, Broggi M, Beer M, et al. Estimation of second-order statistics of buckling loads applying linear and nonlinear analysis. In: Beer M, Zio E, Phoon K-K, Ayyub B, editors. Proceedings of the 8th international symposium on reliability engineering and risk management. 2022, Research Publishing.
- [40] Fina M, Faes M, Valdebenito M, Wagner W, Broggi M, Beer M, et al. Uncertainty quantification of buckling loads of thin and slender structures applying linear and nonlinear analysis. In: 14th international conference on applications of statistics and probability in civil engineering. 2023, URL <http://hdl.handle.net/2262/103597>.
- [41] Fina M, Lauff C, Faes M, Valdebenito M, Wagner W, Freitag S. Bounding imprecise failure probabilities in structural mechanics based on maximum standard deviation. *Struct. Saf.* 2023;101. 102293.
- [42] Freitag S, Edler P, Kremer K, Meschke G. Multilevel surrogate modeling approach for optimization problems with polymorphic uncertain parameters. *Internat J Approx Reason* 2020;119:81–91.
- [43] Hansen P, Pereyra V, Scherer G. Least squares data fitting with applications. Baltimore: Johns Hopkins University Press; 2013.
- [44] Sobol' I. Sensitivity estimates for nonlinear mathematical models.. *Math Model Comput Exper* 1993;18(2):115–55.
- [45] Sobol' I. Theorems and examples on high dimensional model representation. *Reliab Eng Syst Saf* 2003;79(2):187–93.
- [46] Rabitz H, Alis O. General foundations of high-dimensional model representations.. *J Math Chem* 1999;25(2):197–233.
- [47] Rabitz H, Alis O, Shorter J, Shim K. Efficient input-output model representations.. *Comput Phys Comm* 1999;117(1):11–20.
- [48] Kennedy J, Eberhart R. Particle swarm optimization. In: Proceedings of iCNN'95 - international conference on neural networks, vol. 4. 1995, p. 1942–8.
- [49] Bachmann H. Schwingungsprobleme bei Fußgängerbauwerken. *Bauingenieur* 1988;63:67–75.
- [50] Bachmann H. Vibration problems in structures practical guidelines. Birkhäuser Basel; 1995, p. 234.
- [51] Matsumoto Y, Sato S, Nishioka T, Shiojiri H. A study on dynamic design of pedestrian over-bridges. *Trans Japan Soc Civil Eng (JSCE)* 1972;(4):50–1.
- [52] Kramer H, Kebe HW. Durch menschen erzeugte bauwerksschwingungen. *Bauingenieur* 1979;(54):195–9.
- [53] European Coal and Steel Community (ECSC). Generalisation of criteria for floor vibrations for industrial, office, residential and publicbuilding and gymnastic halls. European Commission – Technical Steel Research; 2006.
- [54] Pachi A, Ji T. Frequency and velocity of people walking. *Struct Eng* 2005;83(3):36–40.
- [55] Petersen C, Werkle H. Dynamik der baukonstruktionen. Springer Fachmedien Wiesbaden; 2017.
- [56] Butz E. Beitrag zur Berechnung fußgängerinduzierter Brückenschwingungen. Rheinisch-Westfälische Technische Hochschule Aachen, Fakultät für Bauingenieurwesen; 2006.
- [57] Fischer B, Sedlmeier AM, et al. Anthropometrische messungen in der NAKO gesundheitsstudie – mehr als nur größe und gewicht. *Bundesgesundheitsblatt - Gesundheitsforschung - Gesundheitsschutz* 2020;63(3):290–300.
- [58] DIN EN 1990:2021 eurocode - basis of structural and geotechnical design. 2021, DIN-Normenausschuss Bauwesen (NABau).
- [59] Schuëller G. On the treatment of uncertainties in structural mechanics and analysis. *Comput Struct* 2007;85(5–6):235–43.